Review Received: 2024-01-02, Accepted: 2024-03-28

Elucidating electrochemical energy storage performance of unary, binary, and ternary transition metal phosphates and their composites with carbonaceous materials for supercapacitor applications

Muhammad Ramzan Abdul Karim[1*,†], Waseem Shehzad[1,†], Khurram Imran Khan[1], Ehsan Ul Haq[2*] and Yousaf Haroon[1]

[1]Faculty of Materials and Chemical Engineering, Ghulam Ishaq Khan Institute of Engineering Sciences and Technology (GIKI), Topi- 23640, Khyber Pakhtunkhwa, Pakistan

[2]Department of Metallurgical and Materials Engineering, University of Engineering and Technology (UET), Lahore-54890, Pakistan

*Corresponding authors: tel.: +92 938 281026 (Ext. 2309); Fax: +92 938 281006

MR Abdul Karim (ramzan.karim@giki.edu.pk / ramzan1109@hotmail.com) and EU Haq (amonehsan@uet.edu.pk)

† Authors with equal contribution and sharing first authorship

DOI: 10.33961/jecst.2024.00024

Elucidating electrochemical energy storage performance of unary, binary, and ternary transition metal phosphates and their composites with carbonaceous materials for supercapacitor applications

Abstract

Transition metal compounds (TMCs) are being researched as promising electrode materials for electrochemical energy storage devices (supercapacitors). Among TMCs, transition metal phosphates (TMPs) have good, layered structures owing to open framework and protonic exchange capability among different layers, good surface area due to engrossed porosity, rich active redox reaction sites owing to octahedral structure and variable valance metallic ions. Hence TMPs become more ideal for supercapacitor electrode materials compared to other TMCs. However, TMPs have got some issues like low conductivity, rate performance, stability, energy, and power densities. But these problems can be addressed by making their composites with carbonaceous materials e.g., carbon nanotubes (CNTs), graphene oxide (GO), graphitic carbon (GC) etc. A few factors like high surface area, excellent electrical conductivity of carbon materials and variable valence metal ions in TMPs caused great enhancement in their electrochemical performance. This article tries to discuss and compare the published data, majorly in last decade, regarding the electrochemical energy storage potential of pristine unary, binary, and ternary TMPs and their hybrid composites with carbonaceous materials (CNTs, GOs/rGOs/, GC etc.). The electrochemical performance of the hybrids has been reported to be higher than the pristine counterparts. It is hoped that the current review will open a new gateway to study and explore the high performance TMPs based supercapacitor materials.

Keywords: Transition metal phosphates layered mesoporous structures, carbonaceous materials, supercapacitors, energy storage.

1. Introduction

With advancements in industry and commercial sector, there are many factors which create hindrance in their fast growth in which energy shortage is a serious problem. There are many sources for energy production and used different pollution causing fuels like fossil fuels, biomass, and furnace oil. These energy resources produce electricity but mostly energy is not stored properly due to wastage of these fuels. This energy storage is very useful for small electronic instruments and electric vehicles (EV), Li-ion batteries (LIBs) [1],[2]. LIBs have many limitations i.e., risk for environment due to explosive nature of

DOI: 10.33961/jecst.2024.00024

lithium and hazardous effects of fossil fuels. Among energy storage devices, supercapacitors performed better than classical LIBs and simple capacitors because of good combination of energy and power densities along with good capacity retention especially in case of asymmetric super capacitors (ASC). They are the combination of both pseudo capacitors (PD) (battery like properties) and electric double layer capacitors (EDLC) (capacitor like properties) [3–5] .

Supercapacitors used expensive noble metals active materials like ruthenium oxide (RuO_2), iridium oxide (IrO_2), lithium cobalt oxide ($LiCoO_2$), lithium Iron phosphate ($LiFePO_4$) and platinum / Carbon (Pt/C) which limit their commercial use on the large scale [6–12]. There are different factors like size, porosity and conductivity which control the electrochemical performance [13, 14]. The low cost, abundant nature of hierarchical nanomaterials with good surface area are more appealing for energy storage applications. The structures which have many pores have good faradic reaction due to the reason that they have which more active electrochemical reaction sites [15, 16]. Nanoporous solids having porosity dimensions from meso- (2–50 nm), micro- (<2 nm), to macropores (>50 nm), can lodge and serve as host for metallic atoms, ions for ideal faradic reaction [17–19]. Particularly the mesoporous materials can serve as ideal electrochemically active materials due to tunable porosity, large void space, and highly exposed surface area. Due to these excellent properties, mesoporous materials can efficiently be used in many novel applications like biotechnology, sensors, adsorption/separation, energy storage and conversion [20–27]. The two most thoroughly researched mesoporous compositions since 1990s are organosilicas and periodic mesoporous silicas i.e., sulfides and oxides (PMSs and PMOs) [28–31]. However, apart from the expensive and short range of organosilane coupling molecules, their use in energy storage and conversion applications can be hindered owing to their insulating nature. For this, the non-siliceous mesoporous materials proved to be more commendable materials due to assorted chemistry and functionality [32–34]. Metal phosphates, phosphides, and phosphonates are good potential non-siliceous mesoporous materials due to good structural and electrochemical properties. Metal phosphates seeks significant attention to be used as active catalysts due to good acidic and redox behavior at high rates [35–37].

Different transition metal phosphates (TMPs) (Ni, Mn, V, Zr etc.) have intriguing properties like layered structures with open framework let the proton of acidic group to diffuse through the inter spacing between the layers which make them good conductor for protonic exchange and intercalation of metallic ions [38–40]. Additionally, variable valences of metallic ions could increase the faradic redox reaction. Metal phosphonates have metals linked with phosphonic binders at molecular level [41–43]. Phosphonic acids and the linked compounds have more potential to be bond with different metallic ions. Organic and inorganic molecules linkages results in formation of P-O-M (M = metal) bonds which leads to excellent stable chemical and thermal structures [44–46]. The diverse phosphorus group facilitates its

DOI: 10.33961/jecst.2024.00024

functionalization with different types of functional groups. Their practical use can be enhanced due to modulation of phosphonic group with different functional groups with tailored desirable properties [47–51]. There are other phosphonic group materials like metal phosphides formed by metallic bonds of phosphorus and metallic elements. The novel features of metal phosphides are metalloid and ceramic properties which endorsed effective thermal and chemical stability, good mechanical strength, excellent heat and electric conductivity [52–57]. These all stated factors make transition metal phosphates more distinctive as compared to metal oxides [58, 59]. Additionally, they have other features like good catalytic properties in water splitting and ever-lasting stability [60–62]. These important properties make them most favorable for electrochemical capacitors and batteries. Different heteroatoms TMPs reported in literature like ammonium metal phosphates (AMPs), $NH_4MPO_4.H_2O$ (M = Co^{2+}, Ni^{2+}, Fe^{2+}, and Mn^{2+}) [63–68], $Mn_3(PO_4)_2$, $Ni_3(PO_4)_2$, $VOPO_4$ etc. [69, 70] can be used for energy conversion and storage applications. The reasons for these properties are good electrochemical properties, effective electrical stability and nanostructures favorable for ionic mobility in different sodium/lithium metal phosphates ($NaFePO_4$, $LiMnPO_4$, $LiFePO_4$, and $LiNiPO_4$) for batteries [71–74]. AMPs have highly conductive sheets which are produced by slanted corners of MO_6 with good interconnected NH_4^+ and PO_4^{3-} ions through hydrogen bonding. This will results in good faradic reaction in between inorganic sheets and efficient metallic ions intercalations with a lot of electrochemical reaction sites [70]. TMPs have excellent electrochemical properties in term of energy efficiency, environmental friendliness, structural integrity and safety evaluation as compared to transition metal oxides (TMOs) and hydroxides (TMHs) [15, 17, 18]. Like equally arranged olivine structure with general formula $LiMPO_4$ (M = Fe, Co, Mn, or Ni) has been used on large scale as cathode materials in batteries. Oxygen octahedral sites engaged by other metal ions produced due to durable and strong covalent bonding in tetrahedral anions $(XO_4)_n$ [20]. Lithium-manganese and Lithium-iron based phosphates have been identified as potential positive ions in the olivine structure among the various metal atom replacements. This is primarily because it is inexpensive, environmentally inert, stable while cycle, and highly reversible.

Contrary to many important merits, TMPs have many different drawbacks like low structural integrity, less durability which induced many unfortunate features like phase transformation, limited cyclic life, less structural stability, and electrical conductivity [55, 75, 76]. These unfavorable factors completely influence electrochemical properties of all composites and can be fixed by inducing mesoporosity, effective rate capability, effective electrical and thermal conductivity, greatly exposed surface area and impressive cyclic behavior [13]. These factors along with mechanical and thermal properties can be endorsed by incorporating carbonaceous materials like reduced graphene oxides (rGO), multi-walled carbon nanotubes (MWCNTs) and graphitic carbons (GC) [77–81]. Additionally, specific capacity, energy of TMPs and carbonaceous materials are not too high due to their capacitive behavior which can be catered by functionalization of

DOI: 10.33961/jecst.2024.00024

MWCNTs, rGO, and GC with conducting polymers like polyaniline (PANI) (highest theoretical capacitance of 3407 F g^{-1}), polystyrene (PS), polypropylene (PPY), and other conducting polymers [82, 83]. This can be achieved by formation of more stable and durable functionalization with conducting polymers along with reversible pseudocapacitive behavior and impressive rate capability [82, 84]. Although there are few reviews on different TMPs, but to the authors knowledge there has been no review on TMPs/carbon-based materials which will be very helpful for opening the era for practical research with excellent combination of electrochemical properties. This review article extensively reviews the maximum available studies discussed in literature related to unary, binary, and ternary TMPs and their composites with MWCNTs, reduced graphene oxide (rGO) and other carbon-based materials.

2. Unary metal phosphates / carbon based supercapacitors

UMPs are the single transition metal (Ni, Co, Zn, V) phosphates. Metal phosphates have low conductivity, surface area, porosity which results in their low electrochemical properties. But when their hybrids with carbonaceous materials (CNTs, GRA) then their surface area, conductivity, porosity increased which results in increased electrochemical performance. Following is the comparison electrochemical performance of pristine UMPs and their hybrids.

a. Unary metal phosphate/ Carbon nanotubes (UMP/CNTs) based supercapacitors

Many of the researchers have done considerable reasearch regarding the effect of caboinaceous materials on electrochemcial performance of different TMPs. Few examples are given as follows.

Kim et al. [85] synthesized vanadium phosphate @ carbon nanofoams (VPO/CNFs) nanostructures with the help of carbonaceous materials like CNTs which increase the conductivity of the composite. Firstly, the VPO and in-situ grown CNTs were prepared with the help of phytic acid (PA) in CNF matrix by carbonization process **(Fig. 1a)**. This mixture acts as EDLC material. In **Fig. 1b**, the defect free fibers have cylindrical shape due to the formation of VPO @ CNFs fibers through pyrolysis process. This formation was quite difficult because of the brittle carbon matrix. The flexibility in the fibers incorporated due to uniform CNFs and nanoscale vanadium and low crystalline carbon [85]. This all formed more effective symmetrical combination of electrochemical properties in contrary to asymmetric supercapacitor [86–92]. The ring shaped CNTs can clearly be seen on hierarchical VPO @ CNF matrix from reported TEM images. The most critical factor for the formation of in-situ CNTs decorated VPO nanoparticles were temperature and incorporation of PA. The maximum capacitance of CNTs @ VPO @ CNFs reported was 576.1 F g^{-1} at 0.66 A g^{-1}. The symmetric supercapacitor device (SSCD) presented an energy density of 69.1 W h kg^{-1} (at power density of 3.2 kW kg^{-1}) and maintained to 36.0 W h kg^{-1} @ 32.4 kW kg^{-1}. The superior electrochemical results were due to good conductive CNTs forest and VPO @ CNFs [85].

DOI: 10.33961/jecst.2024.00024

Dutta et al. [93] synthesized hydrated vanadyl phosphate ($VOPO_4.2H_2O$) nano sheets-MWCNT via disperssion of 2-propanol in bath sonicator according to previously reported literature [93, 94]. MWCNT-Vanadyl phosphate hybrid films were prepared by dispersion aided with sonication followed by filtration through polyvinylidene fluoride (PVDF) filtration membrane [93]. Then obtained films were peeled off from the PVDF membranes. Scanning electron microscopy (SEM) images of MWCNT -$VOPO_4$ were showed uniformly mixed $VOPO_4$ nanosheets into MWCNT web **(Fig. 1(c, d))**. The values of specific capacitance recorded were 236, 179, 87, and 59 F g^{-1} at 5, 10, 50, and 100 mVs^{-1} scan rates. Specific capacitance of this composite was five times greater than that of MWCNTs [93]. The reason for best performance was due to thorough mixing of $VOPO_4$ into the MWCNT web which produced the hierarchical network for ideal ionic transfer across the electrode and the meso-porosity in the hybrid film which act as active sites for electronic and ionic intercalation [93].

Shehzad et al. [95] synthesized nickel phosphate – MWCNTs (NiP-CNT) through sonochemical assisted synthesis. First, NiP was prepared from nickel chloride ($NiCl_2$. $6H_2O$) and disodium hydrogen phosphate (Na_2HPO_4) with the help of sonication. Prepared composite was motel and pestle with different quantity of MWCNT (10, 30, 50 wt. %) **(Fig. 1e).** SEM image of NiP50CNT50 shown in **Fig. 1f** presented the homogeneous dispersal of MWCNTs in nickel phosphate ($Ni_3(PO_4)_2$). Due to this, the ions and electrons can easily be conducted throughout the electrolyte. This leads to more effective and speedy faradic reaction. The most appropriate quantity was 50 wt. % MWCNTs, but 10, 30 wt. % cause nucleation and clustering of NiP and CNTs in the nanocomposite which results in depreciation of faradic redox reaction. Due to this, NiP50CNT50 presented a high specific capacity of 845 C g^{-1} at 0.6 A g^{-1} from galvanostatic charge discharge (GCD) pretty much greater than pristine NiP (600.6 C g^{-1} at 0.6 A g^{-1}). The representative electrode showed high conductivity and surface area of 32.4 $m^2 g^{-1}$, adsorbed gas volume (168 $cm^3 g^{-1}$), and mesoporosity as indicated by hysteresis in Brunauer-Emmett-Teller (BET) curves. These pores are electrochemically active reaction sites for reaction to take place. Owing to all these validations, the ASC device of NiP50CNT50//AC showed higher energy density of 94 Wh kg^{-1} (@ power density of 10200 W kg^{-1}) along with impressive capacitance retention of 95.5% after 5000 GCD cycles. The superb cyclic performance was due to homogeneous distribution of CNTs in NiP matrix [95].

Sharmila et al. [96] synthesized $MnPO_4 \cdot H_2O$/MWCNT nanocomposite via hydrothermal methods by adding MWCNTs in $C_4H_6MnO_4$ solution in deionized (DI) water with constant stirring in 1:1 ratio. After adding H_3PO_4 and adjusting the PH of solution to 8, the solution was added into stainless steel autoclave and heated at 80 °C overnight. The schematics of all process represented SEM image showed that the MWCNTs have been thoroughly covered the $MnPO_4 \cdot H_2O$ surface. Both are uniformly distributed among each other. The specific capacitance of obtained composite of $MnPO_4 \cdot H_2O$ / MWCNT was 325 F g^{-1} at 2 A

DOI: 10.33961/jecst.2024.00024

g^{-1} which reduced at high current density [96–98]. This might be due to the combined EDLC natured (MWCNTs) and PD ($MnPO_4 \cdot H_2O$) NSs due to less ionic decomposition and enhanced ionic transfer.

Tian et al. [99] synthesized nickel phosphide/carbon nanotube (Ni_2P @ CNT) nanocomposites by microwave irradiation method. Firstly, the mixture of CNTs, Ni $(NO_3)_2.6H_2O$ and phosphorus was prepared thoroughly in the form of powder followed by heating in microwave oven. The nanospheres of Ni_2P @ CNT can be clearly represented by its reported schematic representation. In the SEM image, clearly Ni_2P nano spheres were thoroughly dispersed on CNT without agglomeration and nucleation. This creates uniform conducting channels for the ionic and electronic conduction in which the nickel ions can easily be diffused through CNTs. Large lumps of Ni_2P showed in SEM images due to prolonged heating time of 120s [100, 101]. Small amount of Ni_2P nanoparticles produced at lower microwave power due to the reason that the CNTs can't engross microwaves for producing Ni_2P nanoparticles. This increase in moisture contents results in the incomplete phase transformations of Ni_2P nanoparticles. The SEM image of Ni_2P @ CNT represents hierarchical morphology including many pores and increased surface area which results in excellent electrochemical performance [99]. The Ni_2P @ CNT nanocomposite produced showed superb rate performance (90%) even at high current density of 10 A g^{-1}. ASC device of Ni_2P @ CNT//AC presented good energy density of 33.5 Wh kg^{-1} (@ power density of 387.5 W kg^{-1}). The best electrochemical properties were because of large quantity of pores which acts as the active electrochemical reaction sites [99, 102]. The other reason was enhanced surface area which is ideal for an electrochemical performance (specific capacitance , energy and power densities) [103–105]. Uniform and thorough growth of Ni_2P over CNTs also enhanced the electrochemical performance [99, 106].

To summarize, the electrochemical performance of UMPs pristine has been compared with their hybrid composites with CNTs based on their hierarchical structure, porosity, surface area and conductivity. Among all the reviewed studies, chemically grafted Ni_2P @ CNTs prepared through microwave irradiation method by **Tian et al.** [99] has been found to excellent results. The specific capacitance of Ni_2P @CNTs found to be 854 F g^{-1} at 1 A g^{-1} greater than pristine Ni_2P (418 F g^{-1} @ 1 A g^{-1}) [107]. The major reason for best performance is the strong chemical grafting between metal phosphate and highly conductive CNTs which will facilitate the ideal ionic and electronic conduction. The highest electrochemical performance of hybrid nanocomposites is due to high conduction, good, exposed surface area, and porosity.

Figure 1:

Table 1:

DOI: 10.33961/jecst.2024.00024

b. Unary metal phosphate/graphene (UMP/Gra) based supercapacitors

Iqbal et al. [108] synthesized zinc phosphate (ZnP) with the help of sonochemical method. Firstly, ZnP was prepared by mixing two solutions of di-sodium hydrogen phosphate (Na_2HPO_4) and zinc chloride ($ZnCl_2$). Finally, the prepared solution was added in autoclave followed by heating at 180 ˚C for 24 hours. After that the prepared precipitate was washed with DI water and ethanol many times followed by room temperature drying for 48 hours **(Fig. 2a)**. On the other hand, rGO was prepared by Hummer's method. Then the ZnP-rGO composite was prepared by physical blending of ZnP and rGO. SEM represents the mixture of rod and particle morphology of ZnP and sheet-like structure of rGO **(Fig. 2b)**. The rGO used in different concentrations (30, 50 wt. %), among which 30 wt. % showed the good specific capacitance (278 F g^{-1} at 0.6 A g^{-1}) due to uniform distribution. The reported validation for the best electrochemical performance of ZnP_rGO_30% was the highest porosity and surface area which results in the formation of active electrochemical reaction sites for an easy access of OH-ions. ZnP_rGO_10% and ZnP_rGO_50% has less active reaction sites due to agglomeration of two phases of ZnP and rGO results in inaccessibility of –OH ions lead to worst electrochemical performance [108].

Mirghni et al. [109] synthesized $Mn_3(PO_4)_2$/GF composite through hydrothermal process. In the process, 50, 100, 150 mg GF were dispersed in DI water through sonication. The precursors used were $C_4H_6MnO_4$ and $N_2H_9PO_4$. The finally prepared mixture was filled in autoclave followed by heating at 200 °C for 24 h and then washing and drying **(Fig. 2c)** [109]. SEM image represented that as-synthesized composite consists of GF sheets covered on hexagonal $Mn_3(PO_4)_2$ micro-rods **(Fig. 2d)**. The good specific capacity of $Mn_3(PO_4)_2$/100 mg GF (270 F g^{-1} @ 0.5 A g^{-1}) was due to effective adherence of uniformly deposited GF sheets on $Mn_3(PO_4)_2$ micro rods with stable conduction paths for ionic diffusion [109].

Mahmoud et al. [110] prepared cobalt phosphate / graphene foam ($Co_3(PO_4)_2$/GF) by dispersing GF in DI water with the help of ultra-sonication. The different precursors were NaOH, $H_9N_2O_4P$, Co $(NO_3)_2$. $6H_2O$ and GF. The precursors were mixed thoroughly in the form of solutions and then stirred followed by drying and annealing at 700 ℃ under N_2 atmosphere. Different compositions, ($Co_3(PO_4)_2$ with 10, 20, 30 mg GF) were made according to scheme as presented in **Fig. 2e** [111]. Structural morphology of $Co_3(PO_4)_2$/20mg GF from SEM represents the uniform grain sized metal phosphates and GF sheets **(Fig. 2e).** In the other compositions of 10 and 30 mg GF, little agglomerates of $Co_3(PO_4)_2$ and GF respectively block the reaction sites which hindered the electronic and ionic flow. The presence of GF increased the electrical conductivity and which results in the formation of proper conductive channels ideal for good faradic reaction. The ASC device of $Co_3(PO_4)_2$/20 mg GF//ppAC showed good energy density of 52 Wh kg^{-1} (@ power density of 847 W kg^{-1}), maintained to 21.6 Wh kg^{-1} @ 10 A g^{-1} current density. Notably, ASC has batter electrochemical performance in comparison with previously reported studies i.e. $Co_3(PO_4)_2$//AC (26.6 Wh.Kg^{-1}) [110],

DOI: 10.33961/jecst.2024.00024

$Co_3P_2O_8.8H_2O$//AC (11.9 Wh.Kg^{-1}) [112], $Ni_3(PO_4)_2$/90 mg GF//C-FP (49 Wh.Kg^{-1}) [76], and $Co_3(PO_4)_2.4H_2O$/GF//C-FP (24 Wh Kg^{-1}) [113].

Mirghni et al. [76] prepared nickel phosphate ($Ni_3(PO_4)_2$) through hydrothermal process by dropping $NiN_2O_6.6H_2O$, into $N_2H_9PO_4$ solution with constant stirring followed by transferring the solution into stainless-steel autoclave at 200 ˚C for 24 h. The prepared solution was washed and dried at 60 ˚C for 12 hours. The obtained product consists of $Ni_3(PO_4)_2$ nano-rods structure [76]. Then graphene foam (GF) was prepared through the method reported in literature [109, 113]. In the process, graphene was grown on annealed Ni foam at 1000 ˚C in the hydrogen (H_2) and argon (Ar) atmosphere for 60 min. After that, CH_4 passed through quartz tube for 10 mins. Once the graphene was fashioned on the nickel foam, GF was formed through etching of nickel by dipping graphene fashioned nickel foam in 3.0 M HCl at 80 ˚C. The prepared GF was frequently washed with DI water and then drying at 60 ˚C overnight. After that the $Ni_3(PO_4)_2$/GF composite was prepared by sonicating GF in DI water followed by formation of hybrid composite through previous hydrothermal method as used for the synthesis of $Ni_3(PO_4)_2$. The different compositions with 30, 60, 90 and 120 mg GF were prepared with the same method. The prepared morphologies of $Ni_3(PO_4)_2$/GF composites were studied with SEM. $Ni_3(PO_4)_2$/30 mg GF showed nano-rods but when 90 mg were used then these nano-rods changed into bundle - like morphology. On further increase of GF contents to 120 mg, the clustering starts which results in the worst electrochemical performance. GF was uniformly coated on $Ni_3(PO_4)_2$ surface aided with sonication for many hours in DI water which was the reason for best electrochemical performance of composite. The nano-rods bundles of $Ni_3(PO_4)_2$/GF composite can be clearly represented by high resolution transmission electron microscopy (HRTEM). The polycrystalline nature of composite can be clearly visible through clear diffraction spots (rings) with the help of selected area electron diffraction (SAED) pattern. From HRTEM, the hierarchical channel-like morphology can be clearly visible in composite with 90 mg GF. It can be clearly visible that with increasing the GF contents, the channel like structure increased but in the 120 mg composition the channel like morphology disappears. Cyclic voltammetry (CV) curve of $Ni_3(PO_4)_2$/30 mg GF has high current as compared to pristine $Ni_3(PO_4)_2$. With 60, 90 mg GF composite the area under the curve increased, especially $Ni_3(PO_4)_2$/90 mg GF showed maximum specific capacity of 48 mA h g^{-1} at 0.5 A g^{-1} with 92% capacitance retention after 2000 GCD cycles with 99% columbic efficiency due to good faradic and reversible nature of composite. ASC device of $Ni_3(PO_4)_2$/90 mg GF// C-FP (Fe^{3+}) adsorbed onto polyaniline (PANI) (C-FP) showed good energy density of 49 Wh kg^{-1} @ 499 W kg^{-1} (retained to 21 Wh kg^{-1} @ 9720 W kg^{-1}). Additionally, the ASC device represented capacity retention of 53% after 10,000 cycles. The energy and power densities of ASC device was greater than previously reported results [114–116]. The best presentation of $Ni_3(PO_4)_2$/90 mg GF composite was due to formation of GF nano-rods networks. These

DOI: 10.33961/jecst.2024.00024

networks have pores which were ideal for faradic reaction to takes place. The ASC device has PANI which is good theoretical capacitance (3407 F g^{-1}) [82, 83]. Due to this reason the ASC device has good energy density and stability.

The electrochemical performance analysis of pristine UMPs done in this section, highlights that there are different controlling factors like conductivity, porosity, and surface area which increase the electrochemical performance of the nanocomposites. Among all studies discussed, ZnP – rGO prepared through sonochemical approach by **Iqbal et al.** [108] showed best results where ZnP and rGO were physically blended with each other. The thorough dispersion of all phases in ZnP – rGO 30% presents good specific capacitance of 278 F g^{-1} at 0.6 A g^{-1} greater then pristine ZnP (59.81 F g^{-1}) [108]. This best performance was attributed to the highest porosity and surface area which results in the formation of active electrochemical reaction sites for easy access of OH-ions.

Figure 2:

Table 2:

3. Binary metal phosphate / carbon based supercapacitors

BMPs are the Double transition metal (Ni, Co, Zn, V) phosphates. Double transition metal has good electrochemical properties as compared to UMPs due to more ions available for their diffusion and effective faradic response. But still these metal phosphates have low conductivity, surface area, porosity which results in their low electrochemical properties. But when their hybrids with carbonaceous materials (CNTs, GRA) then their surface area, conductivity, porosity increased which results in increased electrochemical performance. Following is the comparison electrochemical performance of pristine BMPs and their hybrids.

a. Binary metal phosphate / Carbon nanotubes (BMP/CNTs) based supercapacitors

Dang et al. [117] prepared P doped C spheres @ nickel cobalt phosphide nanosheets (P-CSs @ Ni_1-Co_2-P NSs) as illustrated in **Fig. 3a**. In the first step, CSs were formed through hydrothermal carbonization method [118]. The Ni_1-Co_2-OH NSs was grown on CSs through phosphorization to produce P-CSs @ Ni_1-Co_2-P NSs [117]. SEM micrograph of P-CSs @ Ni_1-Co_2-P NSs as shown in **Fig. 3b**, represents the plain surfaced CSs which were interconnected due to ambient temperature (175 °C) of hydrothermal process. The 3D interlocked uniformly gowned Ni_1-Co_2-P NSs on CSs form a network which can be controlled with the help of low hydrothermal temperature (160 °C) [117]. This growth was due to functional groups, like -C=O, COOH, and -OH on CSs surface [119, 120]. After phosphorization, Ni_1-Co_2-P NSs @ CSs turned into P-CSs @ Ni_1-Co_2-P NSs containing mesopores. This specific hierarchical arrangement caused the more effective transport paths for ideal electronic and ionic conduction. Due to this, specific capacitance of P-

DOI: 10.33961/jecst.2024.00024

CSs @ Ni_1-Co_2-P NSs was 1040.3 F g^{-1} at 1 A g^{-1} [117]. Even at 30 A g^{-1}, composite retains its capacitance to 505.5 F g^{-1}.

Shehzad et al. [121] prepared cobalt nickel phosphate/PANI functionalized CNTs (CNP/PANI-CNTs) nanocomposites through sonochemical assisted synthesis with different masses of PANI/CNTs (20 mg, 40 mg, 60 mg, and 80 mg) labeled as CNP20, CNP40, CNP60, and CNP80. CNTs chemically linked with PANI through in situ-polymerization approach. The reported SEM images of pristine CNP and hybrid CNP40 has rectangular plates. When the PANI/CNTs are added then the size of rectangular plates increases but there is no agglomeration and nucleation of precursors as in the case with CNP40 as compared to CNP20, CNP60. Clear triple layered chemically grafted structures were also verified from reported HRTEM image. CNP40 showed maximum specific capacity of 1268 C g^{-1} at 1.5 A g^{-1} current density. ASC device of CNP40 showed good energy density of 87 Wh kg^{-1} @ power density of 680 W kg^{-1} with 100 % capacitance retention after 5000 GCD cycles. The best performance of CNP40 as compared to other samples is due to stable chemical grafted structures free of clusters due to no agglomeration and nucleation of CNP and PANI/CNTs as in the case of CNP20, CNP60, and CNP80 [121][122].

Guo et al. [123] prepared carbon dots (CDs) according to reported study [124] with the help of citric acid, ethylenediamine (EDA) and phosphorus pentoxide (P_2O_5) through hydrothermal approach. The obtained solution was treated with ethanol to produce precipitate through centrifugation followed by washing and vacuum drying at 40 °C for 24 hours. The effect of variable CDs concentrations dispersed in ethanol on structural appearance has been discussed in **Fig. 3c**. **P**recursors used for the formation of hybrid composite of CDs and nickel zinc phosphate (NZP) were $Ni_3(NO_3)_2 \cdot 6H_2O$, $Na_4P_2O_7$, and $Zn(NO_3)_2 \cdot 6H_2O$. The CDs (0-20 mg) dispersed in the former solution through 20 minutes stirring. Then the whole solution prepared was shifted in the autoclave followed by heating at 160 °C for 8 hours. The finally prepared composite was washed and dried to get precipitates. The different compositions (CDs/NZP-0, CDs/NZP-5, and CDs/NZP-20) were made consisting of different masses of CDs from 0-20 mg [123]. The hierarchical structure of CDs/NZP-10 was represented from TEM image (**Fig. 3d**). The reported structure was mulberry-like, with 200-300 nm diameter. The morphology of pristine NZP changed from irregular to mulberry with the addition of CDs. The hybrid composite of 10 mg CDs has no agglomeration which is ideal for effective ionic ad electronic diffusion which results in rich faradic reaction [123]. The specific capacity of CDs/NZP-10 composite electrode was 1885.7 F g^{-1} at 1 A g^{-1}. These good electrochemical properties make the composite more suitable for high performance electrical appliances. The reason for the better electrochemical performance was effective diffusion of OH- ions. Specifically at low current densities, the OH- ions have sufficient time for their diffusion in the electrode's surface high current densities. This results in large increment in the specific capacitance. The ASC device of CDs/NZP-10//AC presents good energy

DOI: 10.33961/jecst.2024.00024

density of 33.7 Wh kg^{-1} (@ 800 W kg^{-1}) which maintained to 12.4 Wh kg^{-1} (@ 8000 W kg^{-1}) with capacity retention of 90.6% after 6000 GCD cycles. This better working of ASC device was due to highly PD nickel, zinc, and excellent conductive carbon dots.

Kao et al. [125] prepared 2D Iron Phosphate sheets through solvothermal process. The sheetes were formed with the aid of organic templates using solvothermal process. The iron chloride was treated with surfactant Sodium Dodecylbenzene Sulfonate (SDBS). Iron phosphate ($FePO_4$) was synthesized through Sodium Borohydride through thermal annealing caused the chemical reaction of metal and phosphate, reduced onto the organic scaffold, results in the formation of uniform phosphate layer **(Fig. 3e)** [125]. Then the $FePO_4$ water suspension was produced by 12h stirring at 90 ˚C. Reported TEM image showed ultra-thin nanosheets of iron phosphates **(Fig. 3e).** $FePO_4$-PPY devices were fabricated by doping with PPY, SDBS and ammonium persulfate (APS). Pyrrole was polymerized onto the $FePO_4$ ink on glass substrate by evaporation followed by treatment of $FePO_4$-PPY film with CNT forest. Prepared silicon substrate was treated with electron beam to form conductive molybdenum layer. The iron and molybdenum alloy formation were stopped by evaporation of iron and aluminum catalyst. Then the prepared substrate was heated in tube furnace results in growth of CNT forest through chemical vapor deposition (CVD) as reported in literature [126]. After stability of furnace at high temperature of 720 ˚C, ethylene, and hydrogen were introduced in 1:7 ratio. At highest temperature, the catalyst nucleates results in the formation of CNT forest. The porous forest was formed by vacuuming it for 20 min. When $FePO_4$ ink was loaded onto CNT forest, it penetrates into the forest [125]. $FePO_4$-PPY, showed the aerial capacitance of 3.6 mF cm^{-2} (3X more in comparison with bare PPY films), and 20.8 mF cm^{-2} in case of $FePO_4$-CNTs (20X times more than bare CNTs). Yet, a unique multiple-precursor approach for synthesizing 2D materials was presented in this study for the low temperature, solution-processed synthesis of 2D $FePO_4$ sheets. These sheets are easily placed onto conductive substances like PPY and CNTs [125].

Figure 3:

Table 3:

Shehzad et al. [127] synthesized nickel-zinc metal phopsphate-polyaniline / carbon-nanotubes (NZP-PANI/CNTs) nanocomposite through soniochemical approach. Firstly the CNTs were fuctionilized with PANI through insitu polymerization techanioque. Then this PANI/CNTs was treated with metal salts with slow addition of sodium hydrogen phosphate (Na_2HPO_4) to produce the NZP-PANI/CNTs nanocomposite. Final product was washed, dried and then calcined. Obtained marphology was flakes like as in the case of pristine NZP which changed to oval shaped nearly uniform plates when 60 mg PANI/CNTs id added in it. This change was owing to hosmogenious chemical linking of metal phosphates on PANI/CNTs which has

DOI: 10.33961/jecst.2024.00024

been further elaborated by reported Fourier transfer infrared (FT-IR) spectroscopic anlaysis discussed further linking of functional groups in between metal phosphates and PANI/CNTs. The composition NZP60 has greater surface area, conductivity and finally good electrochemical performance (specific capacity = 1143 C g^{-1}) as compared to all other samples like NZP, NZP20, NZP40 and NZP80. The resultant NZP60//AC ASC device presented good energy density of 89.2 Wh kg^{-1} at 630 W kg^{-1} with excellent capacity retention and columbic efficiency. The grounds for outperformance of NZP-PANI/CNTs nanocomposite were high surface area, conductivity, porosity and stable chemical grafting of highly pseudocapcitive NZP and PANI on condutive CNTs. The chemcial stability and rate performance of nanocomposite was attributed to CNTs. This all leads to the foramtion of stable conductive paths ideal for electronic and ionic transport which increase the oxidation and reduction reaction and also whole electrochmical performance of electrode and device [127].

Sharmila et al. [128] prepared MWCNTs wrapped nickel manganese phosphate (NMP) via motel/pastel method. The wrapping of MWCNT on NMP was done in different ratios (1:1, 1:3). Field emission scanning electron microscopy (FESEM) images showed small rods of MWCNTs with increased porosity of 10-20 nm length which were grown on NMP surface [128]. Beside the large rods of MWCNTs, there were also small rods associated with the large one. When the MWCNTs were wrapped on the NMP, it results in balls like morphology due to their coagulation. The electrochemical performance of pristine NMP increased by the inclusion of mesoporous MWCNTs rods. Grounds for good performance were good exposed surface area due to porous nano-rods which act as good electrochemical reaction sites [128].

Wang et al. [129] synthesized cobalt nickel phosphate/manganese dioxide/multi-walled carbon nanotubes composites ($CNPMM_{1:1}$) by hydrothermal method. In the process, $NiCl_2{\cdot}6H_2O$, $CoCl_2{\cdot}6H_2O$, and Na_2HPO_4 were mixed in distilled water with continuous stirring for 30 min. Then the different contents of MnO_2 and MWCNTs in the molar ratios of 1:3, 2:3, 1:1, 3:2, 3:1 were prepared by 30 min stirring. The prepared solution was shifted to stain-less steel autoclave followed by high temperature heating. For comparison, CNP was prepared by the same hydrothermal method. SEM analysis revealed the growth of $CNPMM_{1:1}$ and CNP on nickel foam. The hierarchical clustered morphology of CNP containing long hexagonal petals can be clearly seen in reported SEM images. The highly dense hexagonal petals linked together at center produce many sites for electrochemical reaction due to formation of micron sized central hexaprism [129]. By the addition of MWCNTs and MnO_2, the CNP structure changed from flower like hexagon to cuboid-like morphology. The dimensions of these pores were 0.3–0.8 μm (diameter), 2–3 μm (length). During the co-precipitation reaction, this cluster was extended to large micron which obstructs the directional growth of cobalt and increase the stable growth of Ni base unit [130, 131]. The CNPMM exhibited good electrochemical behavior due to high porosity. The capacities of CNP, $CNPMM_{3:2}$, $CNPMM_{1:1}$, $CNPMM_{3:1}$,

DOI: 10.33961/jecst.2024.00024

$CNPMM_{2:3}$, and $CNPMM_{1:3}$ were 2131, 1229, 2334, 1488, 1781, and 1722 mAh g^{-1} respectively. $CNPMM_{1:1}$ showed maximum capacitance values with cyclic performance of 71.6% at 10 A g^{-1} which was the indication of reduction of ionic diffusions on electrode surface at high current density [132]. The reported reason for this performance was less time for –OH ion intercalation into the electrode surface that is at high current density and has sufficient time for ionic diffusion at low current density. This resulted in large charge storage at low current density which makes it potential candidate to be used in high power applications [133]. The other reason for best electrochemical performance of $CNPMM_{1:1}$ was the added effect of MnO_2, CNP, and MWCNTs in phosphates matrix [131].

Yang et al. [134] synthesized N-CNTs @ NiCoP/CoP with hydrothermal method. In first step, the polypyrrole was prepared with oxidation polymerization of pyrrole followed by self-degraded template method. The N-CNTs were produced with the help of pyrolysis of PPy nanotubes (NTs). Later, the Ni-Co-OH in the form of inter-connected nanosheets decorated on N-CNTs through hydrothermal approach. Then N-CNTs@NiCoP/CoP prepared via $NaH_2PO_2{\cdot}H_2O$, N-CNTs@Ni_1-Co_2-OH precursors. TEM images verified the same morphology of N-CNTs and PPy NTs. Reported SEM images showed the CNTs have less diameter as compared to PPy NTs due to thermal treatment of the polymers. Ni_1-Co_2-OH NSs @ N-CNTs prepared through hydrothermal. In the hierarchical structure of N-CNTs @ NiCoP/CoP, cores of N-CNTs linked thoroughly with interlocked NiCoP/CoP results in the formation of uniform core-shelled mesh structure. This type of hierarchical structure results in the highly exposed which facilitates the consistent ionic and electronic diffusion [135]. Due to all the above reasons, hybrid nanocomposite exhibited more capacity of 152 mAh g^{-1} @ 1 A g^{-1}. Particularly the capacity retention was 61% @ 30 A g^{-1} much greater than the other formed compositions [136].

To summarize, the works reviewed on the pristine BMPs and their hybrids with CNTs present the increment in electrochemical performance due to hierarchical structural effects. Among all the reviewed studies in this section the study reported by **Wang et al.** [129] **(**synthesis of $CNPMM_{1:1}$ through hydrothermal approach) showed best specific capacity of 2334 mAh g^{-1} as compared to pristine CNP. The reported reason for this performance was less time for –OH ion intercalation into the electrode surface that is at high current density and has sufficient time for ionic diffusion at low current density. This resulted in large charge storage at low current density which makes it potential candidate to be used in high power applications [133]. The other reason for best electrochemical performance of $CNPMM_{1:1}$ was the added effect of MnO_2, CNP, and MWCNTs in phosphates matrix [131].

DOI: 10.33961/jecst.2024.00024

b. Binary metal phosphate/graphene (BMP/Gra) based supercapacitors

Zhang et al. [137] prepared Nickel-Cobalt Phosphide/Phosphate/Carbon Nanosheets (Ni-Co-P/PO_x/C) composite through hydrothermal approach **(Fig. 4a)**. The precursors used in this study were Ni $(NO_3)_2 \cdot 6H_2O$, poly (vinylpyrrolidone), 2, 5-dihydroxy terephthalic acid (H4-DHBDC), and $Co(NO_3)_2 \cdot 6H_2O$. Solution of all precursors were mixed in N, N-dimethylformamide (DMF). After that this solution was shifted into autoclave and heated at 160 °C for 12 h followed by washing, centrifuging and drying [137]. Then Ni− Co−P/PO_x/C phase was prepared by phosphorization of as prepared NiCo-MOF. Structural morphology can be elaborated by TEM, SEM **(Fig. 4b)** analysis which represents the 2D nanosheets of NiCo-MOF. TEM image represents the composite which was composed of phosphide nanoparticles (NPs) and phosphate phases. The electrochemical properties of nanocomposites increased due to the amorphous nature of phosphates and phosphides [138][139]. The presence of P, Ni, Co, and C in composite was verified by EDX evaluation. The large percentage of C in composite nanosheets was due to pyrolysis process. The capacitance of as synthesized composite was 583 C g^{-1} at 1 A g^{-1} with superior rate performance of 62.73% at 30 A g^{-1} [137]. The good performance was attributed to the nanopores present in the phosphate and phosphide phase due to its amorphous nature.

Fan et al. [140] synthesized $NiCo(PO_4)_3$/GF composition through hydrothermal route **(Fig. 4c)**. The SEM image of $NiCo(PO_4)_3$/GF shown in **Fig. 4d**. First, pristine NiCo $(PO_4)_3$ was prepared through hydrothermal approach with the help of precursors (Ni $(NO_3)_2 \cdot 6H_2O$, $N_2H_9PO_4$, CH_4N_2O, and Co $(NO_3)_2 \cdot 6H_2O$, and NiCo $(PO_4)_3$) followed by washing and drying to get obtained product. Hybrid composite of NiCo $(PO_4)_3$/GF was finally prepared by same method including GF as precurser. The specific capacity of NiCo $(PO_4)_3$/40 mg GF composite was attributed to 86 mAh g^{-1} @ 1 A g^{-1}. The specific capacity deceased at high current density owing to hindered ionic diffusion results in depreciation of faradic reaction on the less active electrode surface [140].

Mirghni et al. [141] prepared NiMn $(PO_4)_2$/GF composite through hydrothermal approach **(Fig. 4e).** Pristine NiMn $(PO_4)_2$ was prepared by adding (NH_4) PO_4, Ni $(NO_3)_2 \cdot 6H_2O$, and Mn $(CH_3Co)_2 .4H_2O$ in DI water and then transferred this solution in autoclave followed by heating at 120 ºC for 3 hours. Then NiMn $(PO_4)_2$/GF was prepared from the same process by adding 20, 40, 80, and 100 mg GF with the precursors used in reported literature [133, 141]. SEM image of NiMn $(PO_4)_2$/GF represented the cubic rods like hierarchical structure which were well organized due to GF in the structure **(Fig. 4f)**. The capacitance of NiMn $(PO_4)_2$/GF was 97 mAh g^{-1} at 0.5 A g^{-1}. The good performance was attributed to combined synergic outcome of highly electroactive pseudocapacitive Mn and Ni [142]. Other reason was the interaction between GF and NiMn $(PO_4)_2$ which facilitates the efficient ionic and electronic diffusion [141].

DOI: 10.33961/jecst.2024.00024

Figure 4:

Table 4:

Raap et al. [143] prepared CG-CNT nanocomposite which showed rectangular CV curves with high resistance as compared to all other hybrids compounds represents capacitive and reversible performance might be due to EDLC behavior. The faradic reaction was not ideal for carbon based materials due to large amount of quinone and phenol bonds [144]. This process is in close approximation with specified amount of CO repelling groups due to P-functional groups results in carbonyl quinones formation. The different nature of electrode materials produced due to the H_3PO_4 addition during the glucose polymerization with highly resistive CV as compared to CG-CNT [143]. The electrochemical performance of chemically activated glucose activated CNTs (AG-CNT_P800) treated at 800 °C showed specific capacitance of 136 F g^{-1} in three electrode assembly and 133 F g^{-1} both @ 2 mV s^{-1} in two electrode assembly. The CV presented regular shape which might be due to Faradaic reaction. The difference between both capacitances was due to the chemical grafting with oxygen which caused the efficient ionic and electronic diffusion [143].

Among all the reviewed studies on BMPs and their hybrids with graphene in this section, Ni-Co-P/PO_x/C composite synthesized through hydrothermal approach by **Zhang et al.** [137] outperformed. The hybrid composite presented good specific capacity of 583 C g^{-1} at 1 A g^{-1} than pristine Ni-Co-P (453 C g^{-1} at 1 A g^{-1}) [145]. The good electrochemical performance was due to nanopores in phosphate and phosphide phase because of its amorphous nature and highly conductive carbon nanosheets.

4. Ternary metal phosphate /carbon based supercapacitors

TMPs are the triple transition metal (Ni, Co, Zn, V) phosphates. Triple transition metal has good electrochemical properties as compared to BMPs and UMPs due to more ions of three metals available for their diffusion and effective faradic response. But still these metal phosphates have low conductivity, surface area, porosity which results in their low electrochemical properties. But when their hybrids with carbonaceous materials (PANI/CNTs) then their surface area, conductivity, porosity increased which results in increased electrochemical performance. Following is the comparison electrochemical performance of pristine TMPs and their hybrids.

a. Ternary metal phosphate /CNTs (TrMP/PANI-CNT) based supercapacitors

Shehzad et al. [146] prepared nickel – cobalt – zinc metal phosphates – PANI/CNTs nanocomposite through sonochemical assisted synthesis of mixed metal phosphate and PANI functionalized CNTs **(Fig. 5a)**. The morphology of NCZP was irregular sized rectangular plates but it changed into oval sized uniform

DOI: 10.33961/jecst.2024.00024

plates with the addition of 100 mg PANI/CNTs (NCZP100) **(Fig. 5b)**. The HRTEM image of NCZP100 represented that there are triple layers of CNTs, PANI and NCZP phosphate. This showed that there is no gap in between layers but they are completely fused with each other conformed the strong bonding between them **(Fig. 5c)**. Further chemical grafting can be elaborated by reported FT-IR and Ramen spectroscopy. In the study PANI act as bridge in between metal phosphate and CNTs **(Fig. 5d**. The NCZP100 showed good electrical conductivity and specific capacity of 1438 C g^{-1} (2397.5 F g^{-1}) @ 1.5 A g^{-1} current density as compared to all other compositions (NCZP, NCZP20, NCZP40, NCZP60, and NCZP130). The resulting ASC device of NCZP100//AC showed excellent energy density of 104 Whkg^{-1} @ 540 Wkg^{-1} with excellent cyclic performance [146]. The good behavior of NCZP100 and its ASC device was attributed to following reasons:

1) Mixed metal (Ni-Co-Zn) phosphates increase the availability of electrons for oxidation and reduction reactions as all metals have variable oxidation states.
2) High surface area, chemical stability, porosity, and low resistances, conductivity.
3) Stable chemical grafting of highly pseudo-capacitive ternary metal phosphates, PANI and CNTs explained by presence of many functional groups characterized by FT-IR analysis.
4) The best ASC performance was due to all above reasons and combined contribution of pseudo (NCZP60) and EDLC (AC) as indicated by diffusive capacitive performance at different scan rates.

Figure 5:

5. Influences of morphological features, porosity, and surface area on electrochemical performance of pristine TMPs and their hybrids with carbonaceous materials

A few important factors like surface area, conductivity, pore size are certain physiochemical properties affect the electrochemical performance of supercapacitors. Here in this section, it has been tried to discuss the effect of electrochemical performance of different unary, binary, and ternary metal phosphates with the combination of carbon-based materials. This performance is due to hierarchical structures which engrossed good porosity and increased surface area with the inclusion of carbon-based materials. **Table 5** discussed the some studies like nanosheets of $MnPO_4 \cdot H_2O$/MWCNT have high surface area of 19.6 m^2/g and 20 nm pore size as compared to pristine $MnPO_4 \cdot H_2O$ (11.8 m^2/g) with pore size of 17.7 nm [96]. NiP50CNT50 has highest surface area (32.2 m^2/g) [95] as compared to pristine $Ni_3(PO_4)_2$ (16.98 m^2/g) [147]. Nickel phosphates on rGO sheets mesoporous hierarchical structure of $Ni_3(PO_4)_2$/rGO-300 has greater surface area (198.72 m^2/g) [148] than pristine $Ni_3(PO_4)_2$ (16.98 m^2/g) nanosheets [147]. NMP balls wrapped on MWCNTs nanosheets has high surface area of 285.4 m^2/g than pristine NMP (209.2 m^2/g) and low pore size with pore size of 13.2 nm then pristine (18 nm) [128]. Flower like micro cuboid mesoporous structure

DOI: 10.33961/jecst.2024.00024

of $CNPMM_{1:1}$ has greater surface area of 11.7 m^2/g then flower like micro hexagonal structure pristine CNP (5.3 m^2/g) and high porosity (29.4 nm) as compared to pristine CNP (8.7 nm) [131]. These different mesoporous morphologies like nanosheets, nanorods, and flower like microsphere have increased porosity, surface area, conductivity. These porous sites act as electrochemical reaction sites which increase the ionic diffusion resulted in increased oxidation and reduction reactions results in increment of electrochemical performance. Due to all these reasons hybrid metal phosphates/carbonaceous materials have good electrochemical properties in comparison to their relative pristine.

Table 5:

6. Discussion and graphical comparison of the reviewed studies

Current section is presented a comprehensive discussion about the reported studies on different unary, binary and ternary metal phospahtes with CNTs and graphene based materials. This discussion is the comprehensive comparison of hybrid composite of TMPs and carbon based materials with their pristine materials. **Fig. 6** represents all objectives which have been attained in this review article. **Fig. (7-9)** represents specific capacity, energy and power desities and cyclic performances comparison of all hybrid composite electrodes and their representative SSC and ASC devices with their respective pristine materials. **Sharmila et al.** [96] synthesized $MnPO_4 \cdot H_2O$/MWCNT nanocomposite**.** The reported specific capacity was 765 Fg^{-1} pretty much greater then pristine $MnPO_4 \cdot H_2O$ (145 Fg^{-1}) [149]. The electrochemical performance of SSC was 15 Wh kg^{-1} and 350 W kg^{-1} with capacitance retention of 94% after 5000 cycles greater then pristine $MnPO_4$//AC (14.89 Wh kg^{-1} and 1400 W kg^{-1}; 88.9% after 5000 cycles) [150]. The good electrochemical results were due to highly conductive MWCNT. The batter SSC performance was attributed to combined EDLC and pseudo capacitive nature of MWCNTs and $MnPO_4 \cdot H_2O$ NSs respectively due to less ionic decomposition and enhanced ionic transfer [96]. **Dutta et al.** [94] prepared $VOPO_4.2H_2O$/MWCNT through the method explained in previously reported literature. The specific capacitance reported was 236 F g^{-1} at 5 mVs^{-1} scan rate pretty much higher than pristine $VOPO_4$ (202 F g^{-1} at 2 mV s^{-1}) [151]. The reported energy and power densities of nanocomposite were 65.6 Wh kg^{-1} and 1476 W kg^{-1} greater the pristine $VOPO_4 \cdot 2H_2O$ supercapacitor (18.7 Wh/kg @ 290 W/kg) [151]. The reason for best performance was uniform mixing of $VOPO_4$ and MWCNT which formed the hierarchical mesoporous structure ideal for ionic and electronic intercalation [93]. **Tian et al.** [99] prepared Ni_2P @ CNT nanocomposites through microwave irradiation method. The capacitance of 854 F g^{-1} at 1 A g^{-1} more as compared to pristine Ni_2P (418 F g^{-1} @ 1 A g^{-1}) [107]. The ASC device of Ni_2P @ CNT//AC were 33.5 Wh kg^{-1} energy density and 387.5 W kg^{-1} power density with capacitance retention of 84% after 5000 cycles

DOI: 10.33961/jecst.2024.00024

pretty much greater then pristine $Ni_2P_2O_7.8H_2O$//rGO (26.6 Wh kg^{-1} @ 870.6 W kg^{-1} ; 87.35% after 5500 cycles) [152]. The superior electrochemical performance was due to porosity engrossed which have good electrochemical reaction sites [99, 102]. The other reasons were high surface area and uniform growth of Ni_2P over CNTs which is ideal for all electrochemical performance [99, 103–106]. **Shehzad et al.** [95] prepared NiP-CNT nanocomposite via sonochemical synthesis. NiP50CNT50 showed capacity of 845 C g^{-1} at 0.6 A g^{-1} pretty much more as compared to pristine NiP (600.6 C g^{-1} at 0.6 A g^{-1}). The ASC device of NiP50CNT50 showed energy and power densities of 94.5 Wh kg^{-1} and 340 W kg^{-1} with capacity retention of 95.5% after 5000 cycles greater then pristine $Ni_3(PO_4)_2$//AC (26.8 Wh kg^{-1} @ 750 W kg^{-1} ; 87% after 5000 cycles) [153]. The reason for superb electrochemical performance was high conductivity and exposed surface area of 32.4 m^2 g^{-1} owing to combined effect of both NiP and CNTs, adsorbed gas volume (168 cm^3 g^{-1}), and mesoporosity as indicated by hysteresis in BET analysis. These pores act as the active electrochemical reaction sites. The high cyclic performance was due to homogeneous dispersion of MWCNTs. **Mirghni et al.** [76] synthesized $Ni_3(PO_4)_2$/GF through hydrothermal process. $Ni_3(PO_4)_2$/90 mg GF showed more electrochemical performance of 48 mA h g^{-1} at 0.5 A g^{-1} greater than pristine $Ni_3(PO_4)_2$. The electrochemical performance of ASC device of $Ni_3(PO_4)_2$/90mg GF//C-FP was 49 Wh kg^{-1} @ 499 W kg^{-1} and cyclic performance of 92% after 2000 cycles pretty much greater than pristine $Ni_3(PO_4)_2$//AC (26.8 Wh kg^{-1} at 750 W kg^{-1} ; 87% after 5000 cycles) [153]. The best performance was due to GF nano-rods networks having many pores which were ideal for faradic reaction to takes place. **Iqbal et al.** [108] synthesized ZnP with the help of sonochemical method followed physical blending to form ZnP_rGO composite. ZnP_rGO_30% showed 278 F g^{-1} due to uniform distribution much higher than pristine ZnP (59.81 F g^{-1}). The reported causes for the good performance of was due to high porosity and surface area which facilitates faradic reaction for efficient flow of OH-ions, all will lead to effective faradic reaction.

Mirghni et al. [109] prepared $Mn_3(PO_4)_2$/GF composite through hydrothermal route. The more specific capacitance of $Mn_3(PO_4)_2$/100 mg GF (270 F g^{-1} @ 0.5 A g^{-1}) as compared to pristine $Mn_3(PO_4)_2$ (213 F g^{-1} at 5 mV s^{-1}) [154]. The ASC device of $Mn_3(PO_4)_2$/100 mg GF//AC showed 7.6 Wh kg^{-1} and 360 W kg^{-1} with cyclic performance of 96% after 10000 cycles pretty much greater than pristine Mn PO_4//GO (2.271 Wh·kg^{-1} @ 1.5 × 10^5 W·kg^{-1} ; 85.3% after 1000 cycles) [155]. The best performance was attributed to strong bonding of uniformly deposited GF sheets on $Mn_3(PO_4)_2$ micro rods with excellent electrical conductivity. This resulted in increment of specific capacity due to stable conductive paths which facilitate the good metallic ions conduction with electrolyte [109]. **Mahmoud et al.** [111] synthesized $Co_3(PO_4)_2$/GF by dispersion of GF in DI water via ultra-sonication approach with specific capacitance of 57 mAh g^{-1} much greater then pristine $Co_3(PO_4)_2$. The ASC device of $Co_3(PO_4)_2$/20 mg GF//ppAC ASC device showed 24 Wh·kg^{-1} and 468 W·kg^{-1} respectively with cyclic performance of 80% after 10000 cycles batter then pristine $Co_3(PO_4)_2$ (80% after 6000 cycles) and $Co_3P_2O_8.8H_2O$//AC (11.9 Wh kg^{-1} @ 3590 W kg^{-1}) [110].

DOI: 10.33961/jecst.2024.00024

The good performance was due to GF which enhanced electrical conductivity and results in formation of conductive and leads to effective faradic reaction.

Figure 6:

Figure 7 :

Dang et al. [118] prepared P-CSs @ Ni_1-Co_2-P NSs through hydrothermal carbonization method. The specific capacitance of nanocomposites was 1040.3 F g^{-1} at 1 A g^{-1} [117] greater than pristine NCCF-3 (811.1 F·g^{-1} of 1.25 Ag^{-1}) [156]. At high current density of 30 A g^{-1}, it retained to 505.5 F g^{-1}. The ASC device of P-CSs@Ni_1-Co_2-P NSs//AC showed 16.5 Wh kg^{-1} energy density @ power density of 750 W kg^{-1}. The 3D interlocked uniformly gowned Ni_1-Co_2-P NSs on carbon spheres form a network which controlled with the help of low hydrothermal temperature (160 °C) [117]. The causes for batter performance of composite. The reasons for batter electrochemical performance of nanocomposite were presence of many mesopores results in effective transport paths for ideal electronic and ionic conduction. This is all due to transformation of Ni_1-Co_2-P NSs @ CSs into P-CSs @ Ni_1-Co_2-P NSs through phosphorization. **Kim et al.** [85] synthesized VPO/CNFs nanostructures with the help of carbonaceous materials like CNTs. The maximum specific capacitance of CNTs @ VPO @ CNFs composite reported was 576.1 F g^{-1} at 0.66 A g^{-1} more as compared to pristine $VOPO_4$ (~247 F g^{-1} @ 0.5 A g^{-1}). The SSCD device of CNTs @ VPO @ CNFs showed energy density of 69.1 Wh kg^{-1} and 3200 W kg^{-1} with cyclic performance of 109% after 10000 cycles pretty much greater than pristine $VOPO_4.2H_2O$ (18.7 Wh kg^{-1} at 290 W kg^{-1}) [151]. The best electrochemical properties were attributed to increased conductivity of CNTs forest and VPO @ CNFs. **Sharmila et al.** [128] prepared MWCNTs wrapped NMP via mortar/pistol method. The specific capacity of hybrid composite was 812 F g^{-1} @ 2 A g^{-1} greater than pristine NMP (24 F g^{-1}) due to inclusion of mesoporous MWCNTs rods. The ASC device of NMP:MWCNTs//AC presents 78 Wh kg^{-1} and 698 W kg^{-1} with cyclic stability of 90% after 5000 GCD cycles respectively greater then pristine cobalt manganese phosphate//reduced graphene oxide ASC (84% after 6000 cycles) [157] and $NiMn(PO_4)_2$//AC (64.2 Wh kg^{-1} @ 340 W kg^{-1}) [158]. The other reason for better electrochemical performance was highly exposed surface area due to nano-rods with many several pores which act as electrochemically active reaction sites [128]. **Yang et al.** [136] prepared N-CNTs @ NiCoP/CoP through hydrothermal method. The specific capacitance of nanocomposite was 152 mAh g^{-1} @ 1 A g^{-1} greater than pristine NiCoP/CoP (112 mAh g^{-1}). This all was due to thorough interlocked linking of N-CNTs with NiCoP/CoP which results in uniform core-shelled mesh structure with highly exposed surface area and causes more effective ionic and electronic intercalation.

Zhang et al. [137] synthesized Ni-Co-P/PO_x/C through hydrothermal approach. The specific capacity reported was 583 C g^{-1} at 1 A g^{-1} greater then pristine Ni-Co-P (453 C g^{-1} at 1 A g^{-1}) [145]. The ASC

DOI: 10.33961/jecst.2024.00024

device of Ni-Co-P/POx/C//rGO/NF presented electrochemical performance of 35.79 Wh kg^{-1} @ 800 W kg^{-1} with capacitance retention of 83.6% after 5000 cycles more than pristine $NaNi_{0.33}Co_{0.67}PO_4 \cdot H_2O$//Gra (29.85 Wh kg^{-1} @ 374.95 W kg^{-1} ; 76.9% after 10,000 cycles) [159]. The effective electrical properties were due to nanopores in phosphate and phosphide phase because of its amorphous nature and highly conductive carbon nanosheets. **Wang et al.** [131] $CNPMM_{1:1}$ fabricated via hydrothermal approach. The specific capacity of $CNPMM_{1:1}$ was 2334 mAh g^{-1} greater than pristine CNP (2131 mAh g^{-1}). The reported reason for this performance was that at high current density –OH ions have insufficient time for diffusion in electrode surface and at low current density, they have sufficient time for diffusion. This resulted in large charge storage at low current density makes it potential candidate to be used in high power applications [133]. The other reason for best electrochemical performance $CNPMM_{1:1}$ was the added effect of MnO_2, CNP, and MWCNTs in phosphates matrix.

Figure 8 :

Figure 9 :

Fan et al. [140] prepared NiCo $(PO_4)_3$/GF composite through hydrothermal approach. The reported specific capacity of composite was 86.4 mAh g^{-1} greater than pure nickel cobalt phosphate (64 mAh g^{-1}). Electrochemical performance of ASC device to be 34.8 Wh kg^{-1} @ 377 W kg^{-1} with cyclic performance of 95% after 10000 cycles moe than pristine $NaNi_{0.33}Co_{0.67}PO_4 \cdot H_2O$//Gra (29.85 Wh kg^{-1} @ 374.95 W kg^{-1} ; 76.9% after 10,000 cycles) [159]. The batter electrical properties were due to synergic effects of conductive with highly exposed surface area GF and NiCo $(PO_4)_3$. **Mirghni et al.** [142] synthesized NiMn $(PO_4)_2$/GF composite by hydrothermal process. The specific capacity of NiMn $(PO_4)_2$/GF reported was 97 mAh g^{-1} at 0.5 A g^{-1} pretty much higher than NiMn $(PO_4)_2$ (63 mAh g^{-1}) [141]. NiMn$(PO_4)_2$/GF//ppAC ASC device presented energy and power density of 35.42 Wh kg^{-1} and 538 W kg^{-1} respectively with capacitance retention of 97.8% after 10,000 cycles greater than $Mn_3(PO_4)_2$//AC (11.7 Wh kg^{-1} @ 1410 W kg^{-1} ; 99% after 9000 cycles) [149]. The good electrochemical performance was due to combined synergic effect of highly electroactive pseudocapacitive Mn and Ni [142]. Other reason was the interaction between GF and NiMn $(PO_4)_2$ which results in more effective ionic conduction [141]. **Raja et al.** [160] synthesized ZAPG2 with specific capacity of 416 F g^{-1} @ 1 A g^{-1} pretty much greater then pristine pretty much greater then pristine ZAP (328 F g^{-1} @ 1 A g^{-1}).

7. Conclusions

DOI: 10.33961/jecst.2024.00024

Transition metal phosphates (TMPs) have very impressive properties like layered structures with open framework which make them good capable for protonic exchange and ionic intercalation in between different layers. Additionally, variable valencies of metallic ions enhanced the faradic redox reaction. TMPs have good energy efficiency, environmental friendliness, structural integrity, and safety evaluation compared to TMOs and TMHs. Despite some advantages, there are many disadvantages of TMPs like less structural stability, poor capacitance retention, less structural integrity, and electrical conductivity. These demerits can be catered by using TMPs with carbonaceous materials like reduced graphene oxides (rGO), multi-walled carbon nanotubes (MWCNTs), and graphitic carbons (GC). These hybrid materials have mesoporosity, good exposed surface area, layered structure, good conducting paths and excellent cyclic performance. This review comprehensive summarizes all possible reported studies of unary, binary TMPs with carbon-based materials and discuss their electrochemical performance in comparison with the pristine TMPs. These materials have been used in many practical applications like electrical vehicles, electronics appliances etc.

8. Future prospects

Although this review comprehensively discusses hybrid unary, binary, and ternary metal phosphates with carbon-based materials. But in literature there has been no study reported on ternary and quaternary metal phosphates/carbon-based materials. These materials are very important and need to be studied because they will display more effective ionic and electronic intercalation which results in redox rich faradic reaction so good electrochemical performance. Furthermore, the more stable chemical grafting of metal phosphates and carbon – based materials are more useful as compared to physical coupling of precursors. As stable chemical grafting led to batter rate performance and good capacitance retention as compared to physical due to formation of stable functional groups. Second, if we talk about preparation methods, mostly hydrothermal, solvothermal, co-precipitation, sintering, chemical deposition methods and some other methods have been discussed. Bus only one material (NiP50CNT50) prepared by sonochemical approach. This preparation process opens a new gateway in preparing nanocomposites with superb electrochemical performance. The reasons are due to molecular level grafting aided with acoustic cavitation effect. This uniformly formed nanoscale layered structure on molecular level results in very rich faradic reaction due to highest exposed surface area, conduction layered structure which makes these materials potential as positive electrode materials in energy storge devices (supercapacitors) applications.

DOI: 10.33961/jecst.2024.00024

9. References

1. Tarascon JM, Armand M (2010) Issues and challenges facing rechargeable lithium batteries. In: Materials for Sustainable Energy: A Collection of Peer-Reviewed Research and Review Articles from Nature Publishing Group. World Scientific Publishing Co., pp 171–179
2. Li W, Song B, Manthiram A (2017) High-voltage positive electrode materials for lithium-ion batteries. Chem. Soc. Rev. 46:3006–3059
3. Simon P, Gogotsi Y (2008) Materials for electrochemical capacitors. Nat. Mater. 7:845–854
4. Wang G, Zhang L, Zhang J (2012) A review of electrode materials for electrochemical supercapacitors. Chem Soc Rev 41:797–828. https://doi.org/10.1039/c1cs15060j
5. Salunkhe RR, Tang J, Kobayashi N, et al (2016) Ultrahigh performance supercapacitors utilizing core-shell nanoarchitectures from a metal-organic framework-derived nanoporous carbon and a conducting polymer. Chem Sci 7:5704–5713. https://doi.org/10.1039/c6sc01429a
6. Sun M, Liu H, Qu J, Li J (2016) Earth-Rich Transition Metal Phosphide for Energy Conversion and Storage. Adv. Energy Mater. 6:1600087
7. Palomares V, Serras P, Villaluenga I, et al (2012) Na-ion batteries, recent advances and present challenges to become low cost energy storage systems. Energy Environ. Sci. 5:5884–5901
8. Wu G, Zelenay P (2013) Nanostructured nonprecious metal catalysts for oxygen reduction reaction. Acc Chem Res 46:1878–1889. https://doi.org/10.1021/ar400011z
9. Chen L, Xu X, Yang W, Jia J (2020) Recent advances in carbon-based electrocatalysts for oxygen reduction reaction. Chinese Chem Lett 31:626–634. https://doi.org/10.1016/j.cclet.2019.08.008
10. Nie Y, Li L, Wei Z (2015) Recent advancements in Pt and Pt-free catalysts for oxygen reduction reaction. Chem. Soc. Rev. 44:2168–2201
11. Barpanda P, Oyama G, Nishimura SI, et al (2014) A 3.8-V earth-abundant sodium battery electrode. Nat Commun 5:1–8. https://doi.org/10.1038/ncomms5358
12. Tarascon JM (2010) Is lithium the new gold? Nat. Chem. 2:510
13. Baasanjav E, Bandyopadhyay P, Saeed G, et al (2021) Dual-ligand modulation approach for improving supercapacitive performance of hierarchical zinc–nickel–iron phosphide nanosheet-based electrode. J Ind Eng Chem 99:299–308. https://doi.org/10.1016/j.jiec.2021.04.034
14. Khalid W, Abdul Karim MR, Marwat MA (2023) Revolutionizing Energy Storage: Exploring Processing Approaches and Electrochemical Performance of Metal-Organic Frameworks (MOFs) and Their Hybrids. J Electrochem Sci Technol. https://doi.org/10.33961/jecst.2023.00619
15. Thomas A (2010) Functional materials: From hard to soft porous frameworks. Angew. Chemie - Int. Ed. 49:8328–8344
16. Abdul Karim MR, Noman M, Khan KI, et al (2022) Solvothermal Synthesis of Flower-Flakes Like Nano Composites of Ni-Co Metal Organic Frameworks and Graphene Nanoplatelets for Energy Storage Applications. ECS J Solid State Sci Technol 11:011001. https://doi.org/10.1149/2162-8777/ac44f8
17. Davis ME (2002) Ordered porous materials for emerging applications. Nature 417:813–821

DOI: 10.33961/jecst.2024.00024

18. Li W, Liu J, Zhao D (2016) Mesoporous materials for energy conversion and storage devices. Nat. Rev. Mater. 1

19. Abdul Karim MR, Shehzad W (2023) Transition metal compounds and their hybrids with carbonaceous materials for electrochemical energy storage applications. J. Energy Storage 72

20. Ma J, Ren Y, Zhou X, et al (2018) Pt Nanoparticles Sensitized Ordered Mesoporous WO3 Semiconductor: Gas Sensing Performance and Mechanism Study. Adv Funct Mater 28:. https://doi.org/10.1002/adfm.201705268

21. Ghaffar A, Zhang L, Zhu X, Chen B (2018) Porous PVdF/GO Nanofibrous Membranes for Selective Separation and Recycling of Charged Organic Dyes from Water. Environ Sci Technol 52:4265–4274. https://doi.org/10.1021/acs.est.7b06081

22. Yue Q, Wang M, Wei J, et al (2012) A Template Carbonization Strategy to Synthesize Ordered Mesoporous Silica Microspheres with Trapped Sulfonated Carbon Nanoparticles for Efficient Catalysis. Angew Chemie 124:10514–10518. https://doi.org/10.1002/ange.201204719

23. Chen Y, Meng Q, Wu M, et al (2014) Hollow mesoporous organosilica nanoparticles: A generic intelligent framework-hybridization approach for biomedicine. J Am Chem Soc 136:16326–16334. https://doi.org/10.1021/ja508721y

24. Yokoi T, Kubota Y, Tatsumi T (2012) Amino-functionalized mesoporous silica as base catalyst and adsorbent. Appl. Catal. A Gen. 421–422:14–37

25. Mei P, Kim J, Kumar NA, et al (2018) Phosphorus-Based Mesoporous Materials for Energy Storage and Conversion. Joule 2:2289–2306

26. Linares N, Silvestre-Albero AM, Serrano E, et al (2014) Mesoporous materials for clean energy technologies. Chem. Soc. Rev. 43:7681–7717

27. Sun X, Lu L, Zhu Q, et al (2018) MoP Nanoparticles Supported on Indium-Doped Porous Carbon: Outstanding Catalysts for Highly Efficient CO2 Electroreduction. Angew Chemie - Int Ed 57:2427–2431. https://doi.org/10.1002/anie.201712221

28. Hatton B, Landskron K, Whitnall W, et al (2005) Past, present, and future of periodic mesoporous organosilicas - The PMOs. Acc Chem Res 38:305–312. https://doi.org/10.1021/ar040164a

29. Wu SH, Lin HP (2013) Synthesis of mesoporous silica nanoparticles. Chem Soc Rev 42:3862–3875. https://doi.org/10.1039/c3cs35405a

30. Mizoshita N, Inagaki S (2015) Periodic Mesoporous Organosilica with Molecular-Scale Ordering Self-Assembled by Hydrogen Bonds. Angew Chemie - Int Ed 54:11999–12003. https://doi.org/10.1002/anie.201505538

31. Wan Y, Zhao D (2007) On the controllable soft-templating approach to mesoporous silicates. Chem. Rev. 107:2821–2860

32. Schüth F (2001) Non-siliceous mesostructured and mesoporous materials. Chem. Mater. 13:3184–3195

33. Gu D, Schüth F (2014) Synthesis of non-siliceous mesoporous oxides. Chem. Soc. Rev. 43:313–344

34. Ma TY, Yuan ZY (2011) Metal phosphonate hybrid mesostructures: Environmentally friendly multifunctional materials for clean energy and other applications. ChemSusChem 4:1407–1419

DOI: 10.33961/jecst.2024.00024

35. Bhanja P, Chatterjee S, Patra AK, Bhaumik A (2018) A new microporous oxyfluorinated titanium(IV) phosphate as an efficient heterogeneous catalyst for the selective oxidation of cyclohexanone. J Colloid Interface Sci 511:92–100. https://doi.org/10.1016/j.jcis.2017.09.115

36. Conte M, Budroni G, Bartley JK, et al (2006) Chemically induced fast solid-state transitions of ω-VOPO4 in vanadium phosphate catalysts. Science (80-) 313:1270–1273. https://doi.org/10.1126/science.1130493

37. Ren TZ, Yuan ZY, Azioune A, et al (2006) Tailoring the porous hierarchy of titanium phosphates. Langmuir 22:3886–3894. https://doi.org/10.1021/la0533011

38. Murugavel R, Choudhury A, Walawalkar MG, et al (2008) Metal complexes of organophosphate esters and open-framework metal phosphates: Synthesis, structure, transformations, and applications. Chem Rev 108:3549–3655. https://doi.org/10.1021/cr000119q

39. Alberti G, Casciola M, Costantino U, Vivani R (1996) Layered and pillared metal(IV) phosphates and phosphonates. Adv Mater 8:291–303. https://doi.org/10.1002/adma.19960080405

40. Lin R, Ding Y (2013) A Review on the Synthesis and Applications of Mesostructured Transition Metal Phosphates. Mater 2013, Vol 6, Pages 217-243 6:217–243. https://doi.org/10.3390/MA6010217

41. Zhu YP, Ma TY, Liu YL, et al (2014) Metal phosphonate hybrid materials: From densely layered to hierarchically nanoporous structures. Inorg. Chem. Front. 1:360–383

42. Serhan M, Sprowls M, Jackemeyer D, et al (2019) Total iron measurement in human serum with a smartphone. In: AIChE Annual Meeting, Conference Proceedings. pp 1–3

43. Abbas Z, Karim MRA, Shehzad W, et al (2023) Exploring the electrochemical utilization of PANI/CNT-integrated Ni-Mn phosphates for advanced supercapacitor applications. Electrochim Acta 471:143350. https://doi.org/10.1016/j.electacta.2023.143350

44. Gagnon KJ, Perry HP, Clearfield A (2012) Conventional and unconventional metal-organic frameworks based on phosphonate ligands: MOFs and UMOFs. Chem. Rev. 112:1034–1054

45. Vioux A, Bideau J, Mutin PH, Leclercq D (2012) Hybrid Organic-Inorganic Materials Based on Organophosphorus Derivatives. pp 145–174

46. Abdul Karim MR, Khalid W, Zahid R (2024) Comparison of In Situ-Fabricated Ternary NiCoMn-Metal–Organic Frameworks versus Slurry Deposition on Porous Ni-Foam: A Facile Approach for Enhancing Supercapacitor Performance. Energy Technol. https://doi.org/10.1002/ente.202301160

47. Cao G, Hong HG, Mallouk TE (1992) Layered Metal Phosphates and Phosphonates: From Crystals to Monolayers. Acc Chem Res 25:420–427. https://doi.org/10.1021/ar00021a007

48. Mutin PH, Guerrero G, Vioux A (2005) Hybrid materials from organophosphorus coupling molecules. J Mater Chem 15:3761–3768. https://doi.org/10.1039/b505422b

49. Vasylyev M V, Wachtel EJ, Popovitz-Biro R, Neumann R (2006) Titanium phosphonate porous materials constructed from dendritic tetraphosphonates. Chem - A Eur J 12:3507–3514. https://doi.org/10.1002/chem.200501143

50. Clearfield A, Wang Z (2002) Organically pillared microporous zirconium phosphonates. J. Chem. Soc. Dalt. Trans. 2937–2947

51. Freitas FS, Gonçalves AS, De Morais A, et al (2012) Graphene-like MoS2 as a low-cost counter electrode material for dye-sensitized solar cells. This J is © NanoGe J Energy Sustain 11002–

DOI: 10.33961/jecst.2024.00024

11003. https://doi.org/10.1039/c0xx00000x

52. Oyama ST, Gott T, Zhao H, Lee YK (2009) Transition metal phosphide hydroprocessing catalysts: A review. Catal. Today 143:94–107

53. Oyama ST (2008) Transition Metal Carbides, Nitrides, and Phosphides. In: Handbook of Heterogeneous Catalysis

54. Callejas JF, Read CG, Roske CW, et al (2016) Synthesis, Characterization, and Properties of Metal Phosphide Catalysts for the Hydrogen-Evolution Reaction. Chem Mater 28:6017–6044. https://doi.org/10.1021/acs.chemmater.6b02148

55. Li X, Elshahawy AM, Guan C, Wang J (2017) Metal Phosphides and Phosphates-based Electrodes for Electrochemical Supercapacitors. Small 13:1701530

56. Wang M-Q, Ye C, Liu H, et al (2018) Nanosized Metal Phosphides Embedded in Nitrogen-Doped Porous Carbon Nanofibers for Enhanced Hydrogen Evolution at All pH Values. Angew Chemie 130:1981–1985. https://doi.org/10.1002/ange.201710150

57. Lu H, Fan W, Huang Y, Liu T (2018) Lotus root-like porous carbon nanofiber anchored with CoP nanoparticles as all-pH hydrogen evolution electrocatalysts. Nano Res 11:1274–1284. https://doi.org/10.1007/s12274-017-1741-x

58. Ellis BL, Makahnouk WRM, Makimura Y, et al (2007) A multifunctional 3.5V iron-based phosphate cathode for rechargeable batteries. Nat Mater 6:749–753. https://doi.org/10.1038/nmat2007

59. Prosini PP, Lisi M, Scaccia S, et al (2002) Synthesis and Characterization of Amorphous Hydrated FePO[sub 4] and Its Electrode Performance in Lithium Batteries. J Electrochem Soc 149:A297. https://doi.org/10.1149/1.1435359

60. Wang D, Reviews DA-CS, 2017 undefined The recent development of efficient Earth-abundant transition-metal nanocatalysts. pubs.rsc.org

61. Shi Y, Zhang B (2016) Recent advances in transition metal phosphide nanomaterials: Synthesis and applications in hydrogen evolution reaction. Chem. Soc. Rev. 45:1529–1541

62. Xiao P, Chen W, Wang X (2015) A Review of Phosphide-Based Materials for Electrocatalytic Hydrogen Evolution. Adv Energy Mater 5:1500985. https://doi.org/10.1002/aenm.201500985

63. Raju K, Ozoemena KI (2015) Hierarchical one-dimensional ammonium nickel phosphate microrods for high-performance pseudocapacitors. Sci Rep 5:. https://doi.org/10.1038/srep17629

64. Winter S, Tortik N, Kubin A, et al (2013) Back to the roots: Photodynamic inactivation of bacteria based on water-soluble curcumin bound to polyvinylpyrrolidone as a photosensitizer. Photochem Photobiol Sci 12:1795–1802. https://doi.org/10.1039/c3pp50095k

65. Zeng C, Wei W, Zhang L (2012) A general method to prepare metal ammonium phosphate nanoflake constructed microspheres. CrystEngComm 14:3008–3011. https://doi.org/10.1039/c2ce06514b

66. Кирюхина ГВ, Якубович ОВ, Димитрова ОВ (2015) Кристаллическая структура новой полиморфной модификации ниахита NH 4 MnPO 4 · H 2 O. Кристаллография 60:221–226. https://doi.org/10.7868/s0023476115020125

67. Wang Z, Gu J, Liu X, et al (2018) Hierarchical self-assembly flower-like ammonium nickel phosphate as high-rate performance electrode material for asymmetric supercapacitors with

DOI: 10.33961/jecst.2024.00024

enhanced energy density. Nanotechnology 29:425401. https://doi.org/10.1088/1361-6528/aad75f

68. Raju K, Han H, Velusamy DB, et al (2020) Rational Design of 2D Manganese Phosphate Hydrate Nanosheets as Pseudocapacitive Electrodes. ACS Energy Lett 5:23–30. https://doi.org/10.1021/acsenergylett.9b02299

69. Wu C, Lu X, Peng L, et al (2013) Two-dimensional vanadyl phosphate ultrathin nanosheets for high energy density and flexible pseudocapacitors. Nat Commun 4:. https://doi.org/10.1038/ncomms3431

70. Li X, Xiao X, Li Q, et al (2018) Metal (M = Co, Ni) phosphate based materials for high-performance supercapacitors. Inorg. Chem. Front. 5:11–28

71. Kozawa T, Fukuyama K, Kondo A, Naito M (2019) Wet Mechanical Route to Synthesize Morphology-Controlled NH 4 MnPO 4 ·H 2 O and Its Conversion Reaction into LiMnPO 4. ACS Omega 4:5690–5695. https://doi.org/10.1021/acsomega.9b00026

72. Chakraborty I, Bodurtha KJ, Heeder NJ, et al (2014) Massive electrical conductivity enhancement of multilayer graphene/polystyrene composites using a nonconductive filler. ACS Appl Mater Interfaces 6:16472–16475. https://doi.org/10.1021/am5044592

73. Lee KT, Ramesh TN, Nan F, et al (2011) Topochemical synthesis of sodium metal phosphate olivines for sodium-ion batteries. Chem Mater 23:3593–3600. https://doi.org/10.1021/cm200450y

74. Rui X, Zhao X, Lu Z, et al (2013) Olivine-type nanosheets for lithium ion battery cathodes. ACS Nano 7:5637–5646. https://doi.org/10.1021/nn4022263

75. Zhao B, Zhang L, Zhang Q, et al (2018) Rational Design of Nickel Hydroxide-Based Nanocrystals on Graphene for Ultrafast Energy Storage. Adv Energy Mater 8:. https://doi.org/10.1002/aenm.201702247

76. Mirghni AA, Madito MJ, Oyedotun KO, et al (2018) A high energy density asymmetric supercapacitor utilizing a nickel phosphate/graphene foam composite as the cathode and carbonized iron cations adsorbed onto polyaniline as the anode. RSC Adv 8:11608–11621. https://doi.org/10.1039/c7ra12028a

77. Zhong C, Deng Y, Hu W, et al (2015) A review of electrolyte materials and compositions for electrochemical supercapacitors. Chem. Soc. Rev. 44:7484–7539

78. Wang Y, Yu L, Xia Y (2006) Electrochemical Capacitance Performance of Hybrid Supercapacitors Based on Ni(OH)[sub 2]/Carbon Nanotube Composites and Activated Carbon. J Electrochem Soc 153:A743. https://doi.org/10.1149/1.2171833

79. Tao B, Zhang J, Miao F, et al (2010) Preparation and electrochemistry of NiO/SiNW nanocomposite electrodes for electrochemical capacitors. Electrochim Acta 55:5258–5262. https://doi.org/10.1016/j.electacta.2010.04.057

80. Kim YT, Tadai K, Mitani T (2005) Highly dispersed ruthenium oxide nanoparticles on carboxylated carbon nanotubes for supercapacitor electrode materials. J Mater Chem 15:4914–4921. https://doi.org/10.1039/b511869g

81. Butnaru I, Chiriac AP, Constantin CP, Damaceanu MD (2022) Insights into MWCNTs/polyimide nanocomposites: from synthesis to application as free-standing flexible electrodes in low-cost micro-supercapacitors. Mater Today Chem 23:100671. https://doi.org/10.1016/j.mtchem.2021.100671

DOI: 10.33961/jecst.2024.00024

82. Wang YG, Li HQ, Xia YY (2006) Ordered whiskerlike polyaniline grown on the surface of mesoporous carbon and its electrochemical capacitance performance. Adv Mater 18:2619–2623. https://doi.org/10.1002/adma.200600445

83. Aqeel SM, Huang Z, Walton J, et al (2018) Polyvinylidene fluoride (PVDF)/polyacrylonitrile (PAN)/carbon nanotube nanocomposites for energy storage and conversion. Adv Compos Hybrid Mater 1:185–192. https://doi.org/10.1007/s42114-017-0002-5

84. Zhou KL, Wang H, Jiu JT, et al (2018) Polyaniline films with modified nanostructure for bifunctional flexible multicolor electrochromic and supercapacitor applications. Chem Eng J 345:290–299. https://doi.org/10.1016/J.CEJ.2018.03.175

85. Kim H, Prasad Tiwari A, Mukhiya T, Kim HY (2021) Temperature-controlled in situ synthesized carbon nanotube-protected vanadium phosphate particle-anchored electrospun carbon nanofibers for high energy density symmetric supercapacitors. J Colloid Interface Sci 600:740–751. https://doi.org/10.1016/j.jcis.2021.05.090

86. Wang J, He Z, Tan X, et al (2020) High-performance 2.6 V aqueous symmetric supercapacitor based on porous boron doped diamond via regrowth of diamond nanoparticles. Carbon N Y 160:71–79. https://doi.org/10.1016/j.carbon.2020.01.004

87. Owusu KA, Wang Z, Qu L, et al (2020) Activated carbon clothes for wide-voltage high-energy-density aqueous symmetric supercapacitors. Chinese Chem Lett 31:1620–1624. https://doi.org/10.1016/j.cclet.2019.09.045

88. Bhagwan J, Khaja Hussain S, Krishna BNV, Yu JS (2020) β-NiS 3D micro-flower-based electrode for aqueous asymmetric supercapacitors. Sustain Energy Fuels 4:5550–5559. https://doi.org/10.1039/d0se00780c

89. Lokhande AC, Teotia S, Shelke AR, et al (2020) Chalcopyrite based carbon composite electrodes for high performance symmetric supercapacitor. Chem Eng J 399:. https://doi.org/10.1016/j.cej.2020.125711

90. Wei X, Peng H, Li Y, et al (2018) In Situ Growth of Zeolitic Imidazolate Framework-67-derived Nanoporous Carbon@K0.5Mn2O4 for High-Performance 2.4 V Aqueous Asymmetric Supercapacitors. ChemSusChem 11:3167–3174. https://doi.org/10.1002/cssc.201801439

91. Wulan Septiani NL, Kaneti YV, Fathoni KB, et al (2020) Self-assembly of nickel phosphate-based nanotubes into two-dimensional crumpled sheet-like architectures for high-performance asymmetric supercapacitors. Nano Energy 67:. https://doi.org/10.1016/j.nanoen.2019.104270

92. Hosseini H, Shahrokhian S (2018) Advanced binder-free electrode based on core–shell nanostructures of mesoporous Co3V2O8-Ni3V2O8 thin layers@porous carbon nanofibers for high-performance and flexible all-solid-state supercapacitors. Chem Eng J 341:10–26. https://doi.org/10.1016/j.cej.2018.02.019

93. Dutta S, De S (2016) Few layered vanadyl phosphate nano sheets-MWCNT hybrid as an electrode material for supercapacitor application. In: AIP Conference Proceedings. American Institute of Physics Inc.

94. Kim HP, Mohd Yusoff AR Bin, Ryu MS, Jang J (2012) Stable photovoltaic cells based on graphene oxide/indium zinc oxide bilayer anode buffer. Org Electron 13:3195–3202. https://doi.org/10.1016/j.orgel.2012.09.012

95. Shehzad W, Karim MRA, Iqbal MZ, et al (2022) Sono-chemical assisted synthesis of carbon nanotubes-nickel phosphate nanocomposites with excellent energy density and cyclic stability for

DOI: 10.33961/jecst.2024.00024

supercapattery applications. J Energy Storage 54:. https://doi.org/10.1016/j.est.2022.105231

96. Sharmila V, Parthibavarman M (2019) Facile synthesis of MnPO4·H2O nanosheets/MWCNTs composite as electrode material for high-performance supercapacitors. J Mater Sci Mater Electron 30:19813–19825. https://doi.org/10.1007/s10854-019-02347-0

97. Gnana B, Raj S, Wu JJ, et al (2013) Hybrid SnO 2–Co 3 O 4 nanocubes prepared via a CoSn (OH) 6 intermediate through a sonochemical route for energy storage applications. pubs.rsc.org 00:1–3. https://doi.org/10.1039/x0xx00000x

98. Jadhav HS, Pawar SM, Jadhav AH, et al (2016) Hierarchical Mesoporous 3D Flower-like CuCo2O4/NF for High-Performance Electrochemical Energy Storage. Sci Rep 6:. https://doi.org/10.1038/srep31120

99. Tian Y, Du H, Sarwar S, et al (2021) High-performance supercapacitors based on Ni2P@CNT nanocomposites prepared using an ultrafast microwave approach. Front Chem Sci Eng 15:1021–1032. https://doi.org/10.1007/s11705-020-2006-x

100. Yang X, Tian Y, Sarwar S, et al (2019) Comparative evaluation of PPyNF/CoOx and PPyNT/CoOx nanocomposites as battery-type supercapacitor materials via a facile and low-cost microwave synthesis approach. Electrochim Acta 311:230–243. https://doi.org/10.1016/j.electacta.2019.04.084

101. Bi Y, Nautiyal A, Zhang H, et al (2018) One-pot microwave synthesis of NiO/MnO2 composite as a high-performance electrode material for supercapacitors. Electrochim Acta 260:952–958. https://doi.org/10.1016/j.electacta.2017.12.074

102. An C, Wang Y, Li L, et al Effects of highly crumpled graphene nanosheets on the electrochemical performances of pseudocapacitor electrode materials. Elsevier

103. Ding Y, Alias H, Wen D, Williams RA (2006) Heat transfer of aqueous suspensions of carbon nanotubes (CNT nanofluids). Int J Heat Mass Transf 49:240–250. https://doi.org/10.1016/j.ijheatmasstransfer.2005.07.009

104. Wu C, Kopold P, van Aken PA, et al (2017) High Performance Graphene/Ni2P Hybrid Anodes for Lithium and Sodium Storage through 3D Yolk–Shell-Like Nanostructural Design. Adv Mater 29:. https://doi.org/10.1002/adma.201604015

105. Lu Y, Tu JP, Xiong QQ, et al (2012) Controllable synthesis of a monophase nickel phosphide/carbon (Ni 5P 4/C) composite electrode via wet-chemistry and a solid-state reaction for the anode in lithium secondary batteries. Adv Funct Mater 22:3927–3935. https://doi.org/10.1002/adfm.201102660

106. Guang Z, Huang Y, Chen X, et al (2019) Three-dimensional P-doped carbon skeleton with built-in Ni 2 P nanospheres as efficient polysulfides barrier for high-performance lithium-sulfur batteries. Electrochim Acta 307:260–268. https://doi.org/10.1016/j.electacta.2019.03.190

107. Lu Y, Liu JK, Liu XY, et al (2013) Facile synthesis of Ni-coated Ni2P for supercapacitor applications. CrystEngComm 15:7071–7079. https://doi.org/10.1039/c3ce41214h

108. Iqbal MZ, Faisal MM, Ali SR, Afzal AM (2020) Hydrothermally synthesized zinc phosphate-rGO composites for supercapattery devices. J Electroanal Chem 871:. https://doi.org/10.1016/j.jelechem.2020.114299

109. Mirghni AA, Madito MJ, Masikhwa TM, et al (2017) Hydrothermal synthesis of manganese phosphate/graphene foam composite for electrochemical supercapacitor applications. J Colloid

DOI: 10.33961/jecst.2024.00024

Interface Sci 494:325–337. https://doi.org/10.1016/j.jcis.2017.01.098

110. Sankar KV, Lee SC, Seo Y, et al (2018) Binder-free cobalt phosphate one-dimensional nanograsses as ultrahigh-performance cathode material for hybrid supercapacitor applications. J Power Sources 373:211–219. https://doi.org/10.1016/j.jpowsour.2017.11.013

111. Mahmoud BA, Mirghni AA, Oyedotun KO, et al (2020) Synthesis of cobalt phosphate-graphene foam material via co-precipitation approach for a positive electrode of an asymmetric supercapacitors device. J Alloys Compd 818:. https://doi.org/10.1016/j.jallcom.2019.153332

112. Li JJ, Liu MC, Kong L Bin, et al (2015) Facile synthesis of Co3P2O8·8H2O for high-performance electrochemical energy storage. Mater Lett 161:404–407. https://doi.org/10.1016/j.matlet.2015.09.001

113. Mirghni AA, Momodu D, Oyedotun KO, et al (2018) Electrochemical analysis of Co3(PO4)2·4H2O/graphene foam composite for enhanced capacity and long cycle life hybrid asymmetric capacitors. Electrochim Acta 283:374–384. https://doi.org/10.1016/j.electacta.2018.06.181

114. Ma XJ, Zhang W Bin, Kong L Bin, et al (2016) Electrochemical performance in alkaline and neutral electrolytes of a manganese phosphate material possessing a broad potential window. RSC Adv 6:40077–40085. https://doi.org/10.1039/c6ra02217k

115. Liu MC, Li JJ, Hu YX, et al (2016) Design and Fabrication of Ni3P2O8-Co3P2O8·8H2O as Advanced Positive Electrodes for Asymmetric Supercapacitors. Electrochim Acta 201:142–150. https://doi.org/10.1016/j.electacta.2016.03.145

116. Li H, Wang J, Chu Q, et al (2009) Theoretical and experimental specific capacitance of polyaniline in sulfuric acid. J Power Sources 190:578–586. https://doi.org/10.1016/j.jpowsour.2009.01.052

117. Dang T, Wang L, Wei D, et al (2019) Bifunctional phosphorization synthesis of mesoporous networked Ni-Co-P/phosphorus doped carbon for ultra-stable asymmetric supercapacitors. Electrochim Acta 299:346–356. https://doi.org/10.1016/j.electacta.2018.12.176

118. Sun X, Li Y (2004) Colloidal Carbon Spheres and Their Core/Shell Structures with Noble-Metal Nanoparticles. Angew Chemie 116:607–611. https://doi.org/10.1002/ange.200352386

119. Xiao X, Han B, Chen G, et al (2017) Preparation and electrochemical performances of carbon sphere@ZnO core-shell nanocomposites for supercapacitor applications. Sci Rep 7:. https://doi.org/10.1038/srep40167

120. Réti B, Kiss GI, Gyulavári T, et al (2017) Carbon sphere templates for TiO2 hollow structures: Preparation, characterization and photocatalytic activity. Catal Today 284:160–168. https://doi.org/10.1016/j.cattod.2016.11.038

121. Abdul Karim MR, Shehzad W, Atif M, et al (2024) Sonochemically synthesized novel CNTs-PANI/CoNi(PO4)2 nanocomposites with enhanced electrochemical energy storage performance for asymmetric supercapacitor applications. Energy Environ. https://doi.org/10.1177/0958305X231221260

122. Shehzad W, Abdul Karim MR (2024) Exploration of electrochemical energy storage potential of PANI functionalized CNTs/Zn-Co(PO4)2 nanocomposites synthesized via a facile ultrasounds-assisted chemical method. J Energy Storage 81:. https://doi.org/10.1016/j.est.2024.110435

123. Guo M, Wang S, Zhao L, Guo Z (2018) High-performance asymmetric supercapacitor based on

DOI: 10.33961/jecst.2024.00024

flowery nickel-zinc phosphate microspheres with carbon dots. Electrochim Acta 292:299–308. https://doi.org/10.1016/j.electacta.2018.08.119

124. Wei JS, Ding H, Zhang P, et al (2016) Carbon Dots/NiCo2O4Nanocomposites with Various Morphologies for High Performance Supercapacitors. Small 12:5927–5934. https://doi.org/10.1002/smll.201602164

125. Kao E, Jang HS, Zang X, Lin L (2017) Synthesis and integration of 2D Iron Phosphate sheets for energy storage devices. In: TRANSDUCERS 2017 - 19th International Conference on Solid-State Sensors, Actuators and Microsystems. pp 1336–1339

126. Jiang YQ, Zhou Q, Lin L (2009) Planar mems supercapacitor using carbon nanotube forests. In: Proceedings of the IEEE International Conference on Micro Electro Mechanical Systems (MEMS). pp 587–590

127. Shehzad W, Ramzan · Muhammad, Karim A (2023) Synthesis and electrochemical energy storage performance evaluation of PANI functionalized CNTs/Ni–Zn (PO4)2 nanocomposites. Appl Phys A 2023 1297 129:1–17. https://doi.org/10.1007/S00339-023-06732-9

128. Sharmila V, Packiaraj R, Nallamuthu N, Parthibavarman M (2020) Fabrication of MWCNTs wrapped nickel manganese phosphate asymmetric capacitor as a supercapattery electrode for energy storage applications. Inorg Chem Commun 121:108194. https://doi.org/10.1016/j.inoche.2020.108194

129. Rajesh JA, Park JH, Vinh Quy VH, et al (2018) Rambutan-like cobalt nickel sulfide (CoNi2S4) hierarchitecture for high-performance symmetric aqueous supercapacitors. J Ind Eng Chem 63:73–83. https://doi.org/10.1016/j.jiec.2018.02.001

130. Wang L, Zhang R, Jiang Y, et al (2019) Interfacial synthesis of micro-cuboid Ni0.55Co0.45C2O4 solid solution with enhanced electrochemical performance for hybrid supercapacitors. Nanoscale 11:13894–13902. https://doi.org/10.1039/c9nr03790j

131. Wang S wen, Mao M, Cao Y, et al (2020) Novel cuboid-like cobalt nickel phosphate/manganese dioxide/multi-walled carbon nanotubes composites as binder-free electrodes for high-performance supercapacitors. Inorg Chem Commun 114:. https://doi.org/10.1016/j.inoche.2020.107822

132. Theerthagiri J, Thiagarajan K, Senthilkumar B, et al (2017) Synthesis of Hierarchical Cobalt Phosphate Nanoflakes and Their Enhanced Electrochemical Performances for Supercapacitor Applications. ChemistrySelect 2:201–210. https://doi.org/10.1002/slct.201601628

133. Li B, Shi Y, Huang K, et al (2018) Cobalt-Doped Nickel Phosphite for High Performance of Electrochemical Energy Storage. Small 14:. https://doi.org/10.1002/smll.201703811

134. Yang X, Zhu Z, Dai T, Lu Y (2005) Facile fabrication of functional polypyrrole nanotubes via a reactive self-degraded template. Macromol Rapid Commun 26:1736–1740. https://doi.org/10.1002/marc.200500514

135. Khalid W, Abdul Karim MR, Atif M, et al (2023) Ultrasounds-assisted solvothermal synthesis of Ni-Co-Mn MOFs/PANI-CNTs nanocomposites with enhanced electrochemical energy storage performance. Energy Environ. https://doi.org/10.1177/0958305X231196126

136. Dang T, Wei D, Zhang G, et al (2020) Homologous NiCoP/CoP hetero-nanosheets supported on N-doped carbon nanotubes for high-rate hybrid supercapacitors. Electrochim Acta 341:. https://doi.org/10.1016/j.electacta.2020.135988

137. Zhang X, Wang J, Sui Y, et al (2020) Hierarchical Nickel-Cobalt Phosphide/Phosphate/Carbon

DOI: 10.33961/jecst.2024.00024

Nanosheets for High-Performance Supercapacitors. ACS Appl Nano Mater 3:11945–11954. https://doi.org/10.1021/acsanm.0c02507

138. Zahid R, Abdul Karim MR, Khalid W, Marwat MA (2024) Tailoring the Effect of NiCo-Metal-Organic Frameworks by Doping Manganese as a Highly Active Redox Electrode for Electrochemical Energy Storage Technologies: Supercapattery Devices. Energy Technol. https://doi.org/10.1002/ente.202300883

139. Khalid W, Abdul Karim MR, Shahid ASA, et al (2024) Nanocomposites of Ni-Co-Mn MOFs and PANI functionalized CNTs-GNPs with excellent electrochemical performance for energy storage applications. J Energy Storage 77:. https://doi.org/10.1016/j.est.2023.109962

140. Mirghni AA, Oyedotun KO, Mahmoud BA, et al (2019) Nickel-cobalt phosphate/graphene foam as enhanced electrode for hybrid supercapacitor. Compos Part B Eng 174:106953. https://doi.org/10.1016/j.compositesb.2019.106953

141. Mirghni AA, Oyedotun KO, Fasakin O, et al (2020) High-performance bimetallic Ni-Mn phosphate hybridized with 3-D graphene foam for novel hybrid supercapacitors. J Energy Storage 31:101584. https://doi.org/10.1016/j.est.2020.101584

142. Li M, Cheng JP, Wang J, et al (2016) The growth of nickel-manganese and cobalt-manganese layered double hydroxides on reduced graphene oxide for supercapacitor. Electrochim Acta 206:108–115. https://doi.org/10.1016/j.electacta.2016.04.084

143. Rey-Raap N, Granja MAC, Pereira MFR, Figueiredo JL (2020) Phosphorus-doped carbon/carbon nanotube hybrids as high-performance electrodes for supercapacitors. Electrochim Acta 354:. https://doi.org/10.1016/j.electacta.2020.136713

144. Rey-Raap N, Enterría M, Martins JI, et al (2019) Influence of Multiwalled Carbon Nanotubes as Additives in Biomass-Derived Carbons for Supercapacitor Applications. ACS Appl Mater Interfaces. https://doi.org/10.1021/acsami.8b19246

145. Li B, Gu P, Feng Y, et al (2017) Ultrathin Nickel–Cobalt Phosphate 2D Nanosheets for Electrochemical Energy Storage under Aqueous/Solid-State Electrolyte. Adv Funct Mater 27:. https://doi.org/10.1002/adfm.201605784

146. Shehzad W, Abdul Karim MR (2023) Improved energy storage performance of sonochemically synthesized Ni-Co-Zn ternary metal phosphate composites by incorporating PANI functionalized CNTs. Diam Relat Mater 137:. https://doi.org/10.1016/j.diamond.2023.110050

147. Wulan Septiani NL, Kaneti YV, Fathoni KB, et al (2020) Self-assembly of nickel phosphate-based nanotubes into two-dimensional crumpled sheet-like architectures for high-performance asymmetric supercapacitors. Nano Energy 67:. https://doi.org/10.1016/j.nanoen.2019.104270

148. Yuan J, Zheng X, Yao D, et al (2018) Amorphous mesoporous nickel phosphate/reduced graphene oxide with superior performance for electrochemical capacitors. Dalt Trans 47:13052–13062. https://doi.org/10.1039/c8dt02304b

149. Katkar PK, Marje SJ, Pujari SS, et al (2020) Single-pot hydrothermal synthesis of manganese phosphate microrods as a cathode material for highly stable flexible solid-state symmetric supercapacitors. Synth Met 267:116446. https://doi.org/10.1016/j.synthmet.2020.116446

150. Ma XJ, Zhang W Bin, Kong L Bin, et al (2016) Electrochemical performance in alkaline and neutral electrolytes of a manganese phosphate material possessing a broad potential window. RSC Adv 6:40077–40085. https://doi.org/10.1039/c6ra02217k

DOI: 10.33961/jecst.2024.00024

151. Luo Z, Liu E, Hu T, et al (2014) Effect of synthetic methods on electrochemical performances of VOPO4·2H2O supercapacitor. Ionics (Kiel) 21:289–294. https://doi.org/10.1007/s11581-014-1317-7

152. Marje SJ, Katkar PK, Pujari SS, et al (2020) Regulated micro-leaf like nickel pyrophosphate as a cathode electrode for asymmetric supercapacitor. Synth Met 259:. https://doi.org/10.1016/j.synthmet.2019.116224

153. Li N, Xu Z, Liu Y, Hu Z (2019) Hollow amorphous microspheres of nickel phosphate: Synthesis using adenosine 5′′-triphosphate disodium salt as a new organic phosphorus source and their application as electrode materials in supercapacitors. J Power Sources 426:1–10. https://doi.org/10.1016/j.jpowsour.2019.04.016

154. El Mouahid H, Bou-ouzoukni Y, Kaichouh G, et al (2022) Electrodeposition of MnPO4·H2O thin film and their characterization as supercapacitor material by potentiodynamic method. J Energy Storage 50:. https://doi.org/10.1016/j.est.2022.104677

155. Yan B, Bin D, Ren F, et al (2016) Facile synthesis of MnPO4·H2O nanowire/graphene oxide composite material and its application as electrode material for high performance supercapacitors. Catalysts 6:. https://doi.org/10.3390/catal6120198

156. Ma S, Xiang D, Wang Y, et al (2022) Ammonium nickel-cobalt phosphate nanoflowers on highly conductive carbon fibers as an electrode material for enhanced electrochemical performance supercapacitors. Asia-Pacific J Chem Eng 17:. https://doi.org/10.1002/APJ.2749

157. Katkar PK, Marje SJ, Parale VG, et al (2021) Fabrication of a High-Performance Hybrid Supercapacitor Based on Hydrothermally Synthesized Highly Stable Cobalt Manganese Phosphate Thin Films. Langmuir 37:5260–5274. https://doi.org/10.1021/acs.langmuir.1c00243

158. Alam S, Iqbal MZ (2021) Nickel-manganese phosphate: An efficient battery-grade electrode for supercapattery devices. Ceram Int 47:11220–11230. https://doi.org/10.1016/j.ceramint.2020.12.247

159. Liu M, Shang N, Zhang X, et al (2019) Microwave synthesis of sodium nickel-cobalt phosphates as high-performance electrode materials for supercapacitors. J Alloys Compd 791:929–935. https://doi.org/10.1016/j.jallcom.2019.03.382

160. Arul Raja T, Vickraman P, Simon Justin A, Joji Reddy B (2020) Microwave Synthesis of Zinc Ammonium Phosphate/Reduced Graphene Oxide Hybrid Composite for High Energy Density Supercapacitors. Phys Status Solidi Appl Mater Sci 217:. https://doi.org/10.1002/pssa.201900736

161. Kim D, Kang J, Yan B, et al (2020) Ambient Temperature Synthesis of Iron-Doped Porous Nickel Pyrophosphate Nanoparticles with Long-Term Chemical Stability for High-Performance Oxygen Evolution Reaction Catalysis and Supercapacitors. ACS Sustain Chem Eng 8:2843–2853. https://doi.org/10.1021/acssuschemeng.9b06920

162. Ling J, Zou H, Yang W, et al (2019) Self-enhanced electrochemical properties of Ni–P nanosphere with heterogeneous Ni and Ni–P nanoflake outer layer anchored on carbon cloth for asymmetric all-solid-state supercapacitors. J Mater Sci Mater Electron 30:18088–18100. https://doi.org/10.1007/s10854-019-02162-7

163. Li JJ, Liu MC, Kong L Bin, et al (2015) Advanced asymmetric supercapacitors based on Ni3(PO4)2@GO and Fe2O3@GO electrodes with high specific capacitance and high energy density. RSC Adv 5:41721–41728. https://doi.org/10.1039/c5ra06050h

164. Marje SJ, Katkar PK, Pujari SS, et al (2020) Effect of phosphate (anion) precursor on structural

DOI: 10.33961/jecst.2024.00024

and morphology behavior of nickel phosphate thin films and its supercapacitive performance. Mater Sci Eng B Solid-State Mater Adv Technol 261:. https://doi.org/10.1016/j.mseb.2020.114641

165. Peng H, Zhou J, Chen Z, et al (2019) Integrated carbon nanosheet frameworks inlaid with nickel phosphide nanoparticles by substrate-free chemical blowing and phosphorization for aqueous asymmetric supercapacitor. J Alloys Compd 797:1095–1105. https://doi.org/10.1016/j.jallcom.2019.04.301

166. Hao J, Zou X, Feng L, et al (2021) Facile fabrication of core-shell structured Ni(OH)2/Ni(PO3)2 composite via one-step electrodeposition for high performance asymmetric supercapacitor. J Colloid Interface Sci 583:243–254. https://doi.org/10.1016/j.jcis.2020.08.123

167. Marje SJ, Patil V V., Parale VG, et al (2021) Microsheets like nickel cobalt phosphate thin films as cathode for hybrid asymmetric solid-state supercapacitor: Influence of nickel and cobalt ratio variation. Chem Eng J 429:132184. https://doi.org/10.1016/j.cej.2021.132184

DOI: 10.33961/jecst.2024.00024

Figures

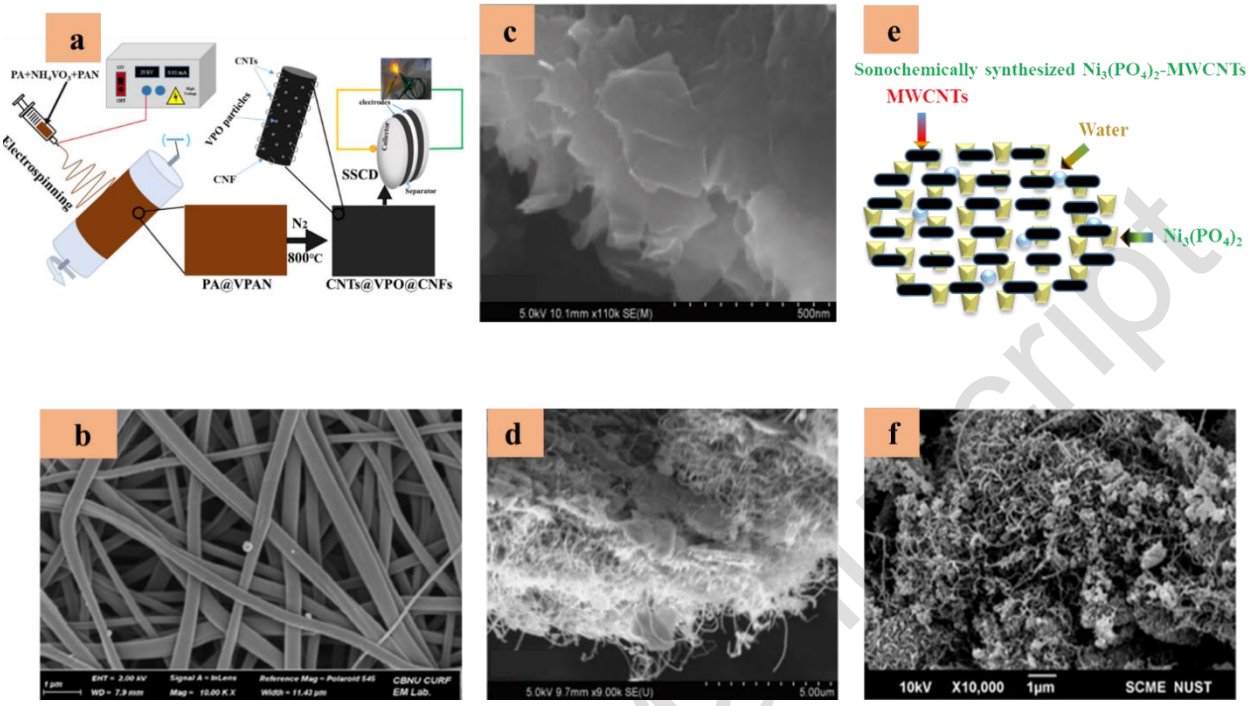

Figure 1: Illustration presented the synthesis and FE-SEM image of symmetric supercapacitors (SSC) of CNTs @ VPO @ CNFs (c, d) [85] **; FESEM images of exfoliated $VOPO_4$ (a), MWCNT-$VOPO_4$ hybrid film (c)** [93]**; schematic representation and SEM image of NiP50CNT50 composite (e, f)** [95] **—reproduced with permission.**

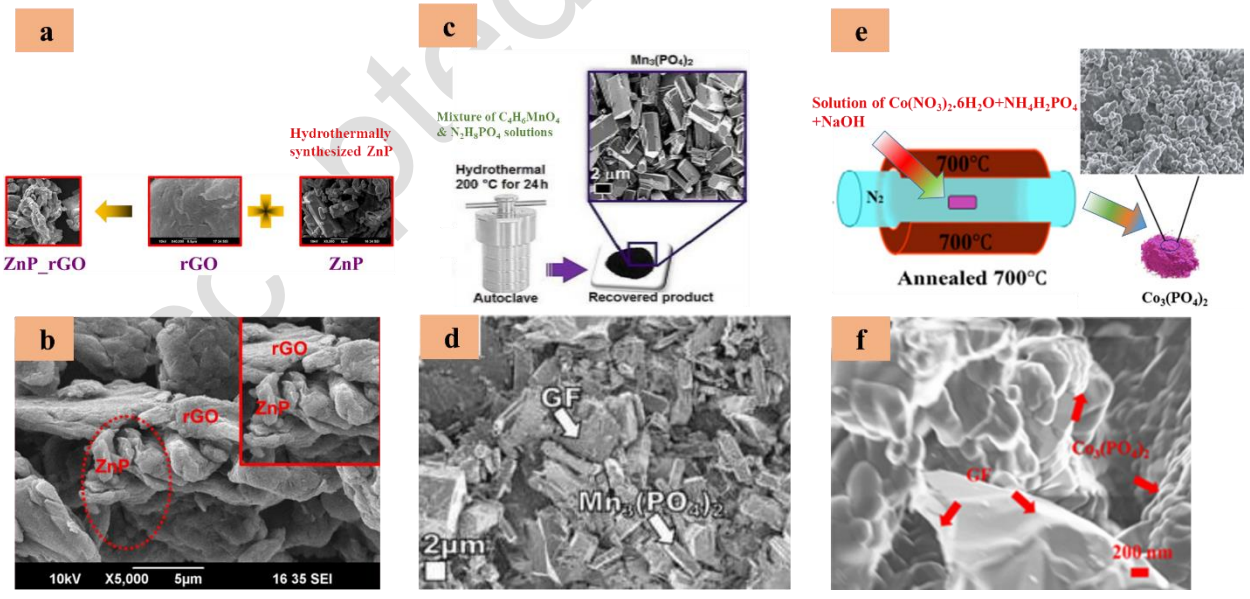

Figure 2: Schematics representation and SEM image of ZnP-rGO composite (a, b) [108] **; Schematic preparation and SEM image of $Mn_3(PO_4)_2$/100 mg GF composite (c, d)** [109] **; Schematic synthesis and SEM image of $Co_3(PO_4)_2$/20 mg GF (e, f)** [111] **— reproduced with permission.**

DOI: 10.33961/jecst.2024.00024

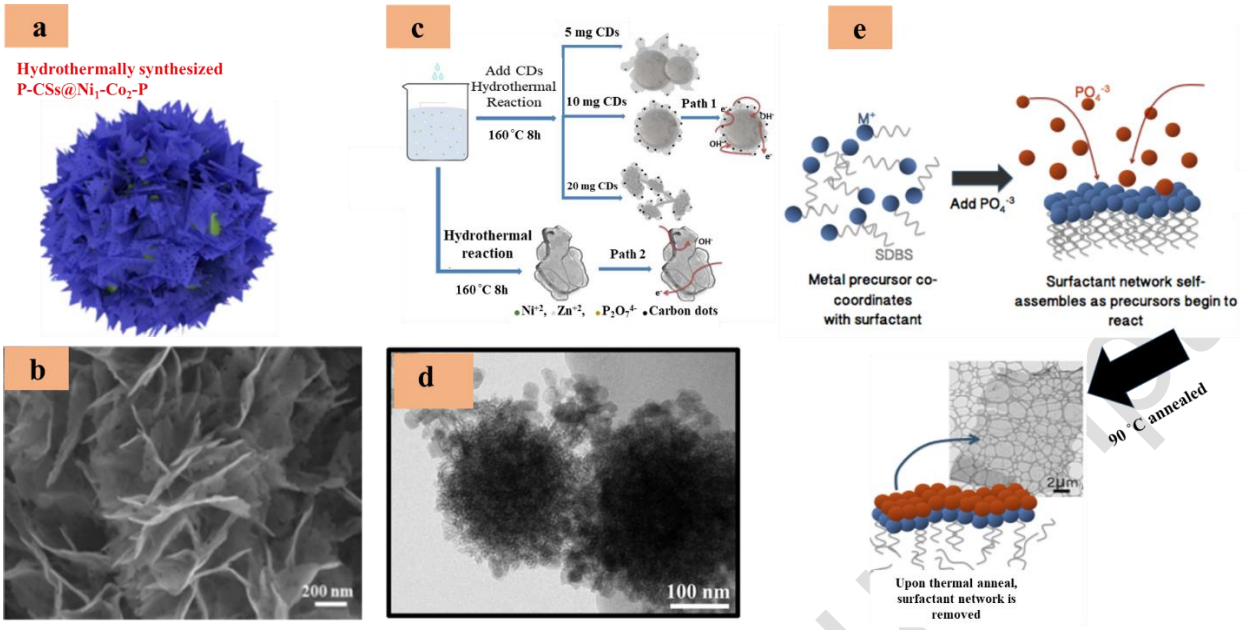

Figure 3: Schematic representation and SEM image of P-CSs@Ni_1-Co_2-P NSs (a, b) [117] **; Schematic presents morphology transformation with the addition of carbon dots in different amounts and electronic diffusion flow path, TEM image of CDs/NZP-10 (c, d)** [123]**; Representation of phosphate self-assembly of $FePO_4$-PPY and $FePO_4$-CNTs . Firstly, different metal precursors reacted with surfactant (SDBS). At 90 ˚C, reduction reaction caused through precursors. (Inset) TEM image of finally formed sheet (e)** [125] **— reproduced with permission.**

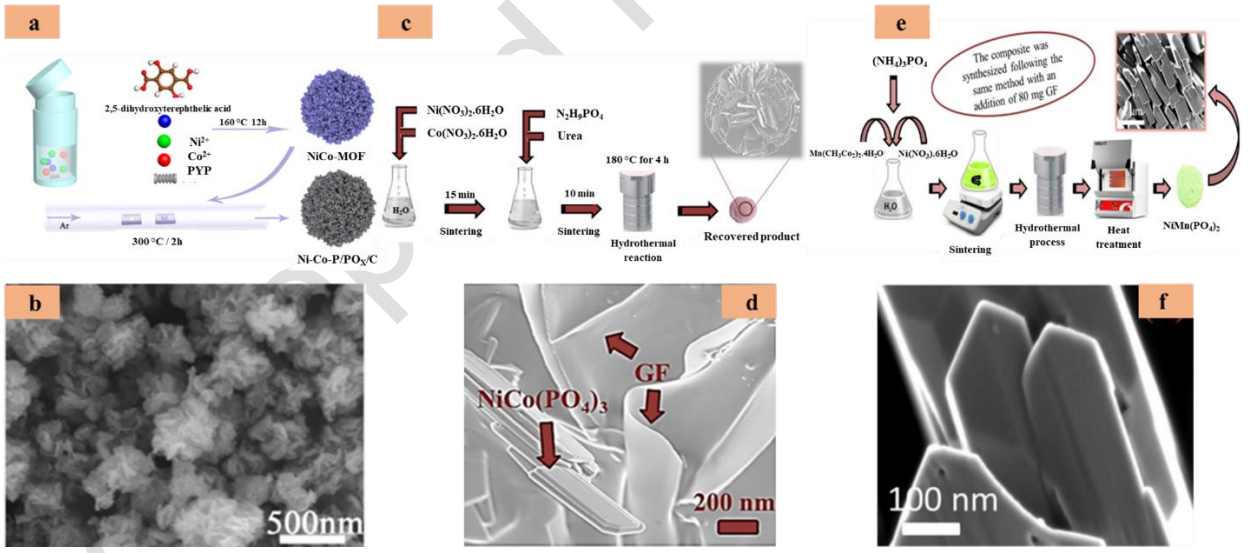

Figure 4: Schematic synthesis and SEM image of bimetallic Ni-Co-P/PO_x/C (a, b) [137] **; Schematic preparation of $NiCo(PO_4)_3$ (c), SEM image of $NiCo(PO_4)_3$/GF (d)** [140]**, schematic synthesis of $NiMn(PO_4)_2$ and $NiMn(PO_4)_2$/GF composite (e) high magnification image of $NiMn(PO_4)_2$/GF(f)** [141] **— reproduced with permission**

DOI: 10.33961/jecst.2024.00024

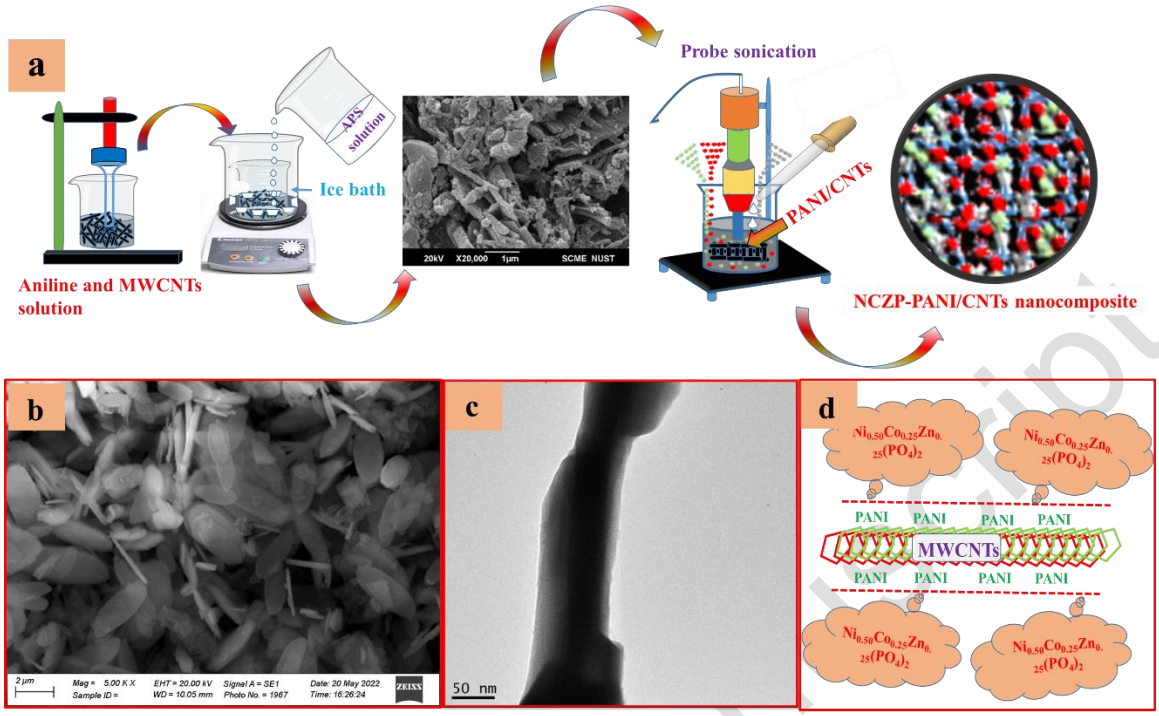

Figure 5: Schematic synthesis of NCZP-PANI/CNTs nanocomposite (a); SEM and HRTEM images of NCZP100 (b, c); and layered mixed metal phosphate – PANI/CNTs nanocomposite (d) [146]**-reproduced with permission**

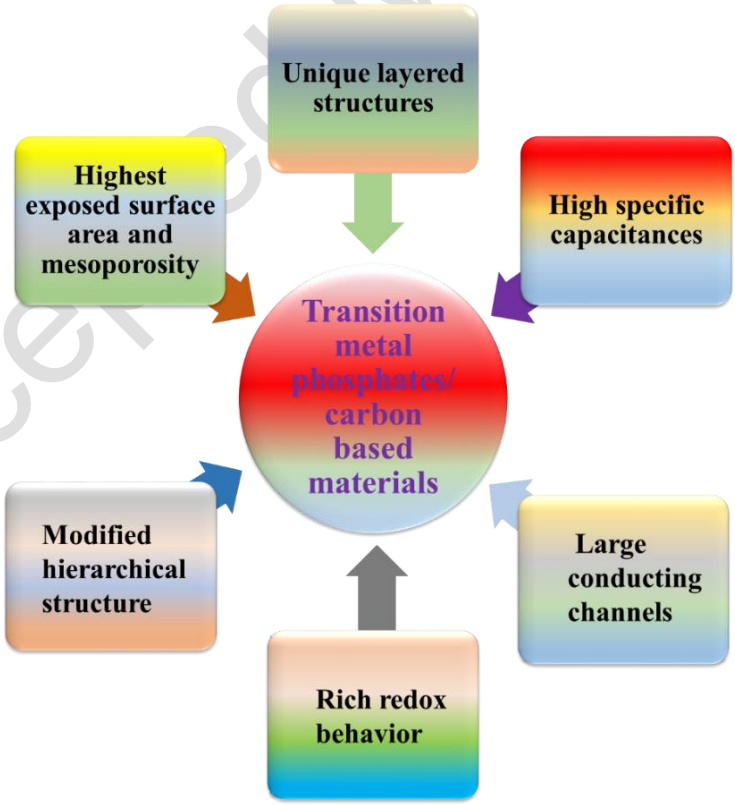

Figure 6: Characteristics of TMPs/Carbon based nanocomposites

DOI: 10.33961/jecst.2024.00024

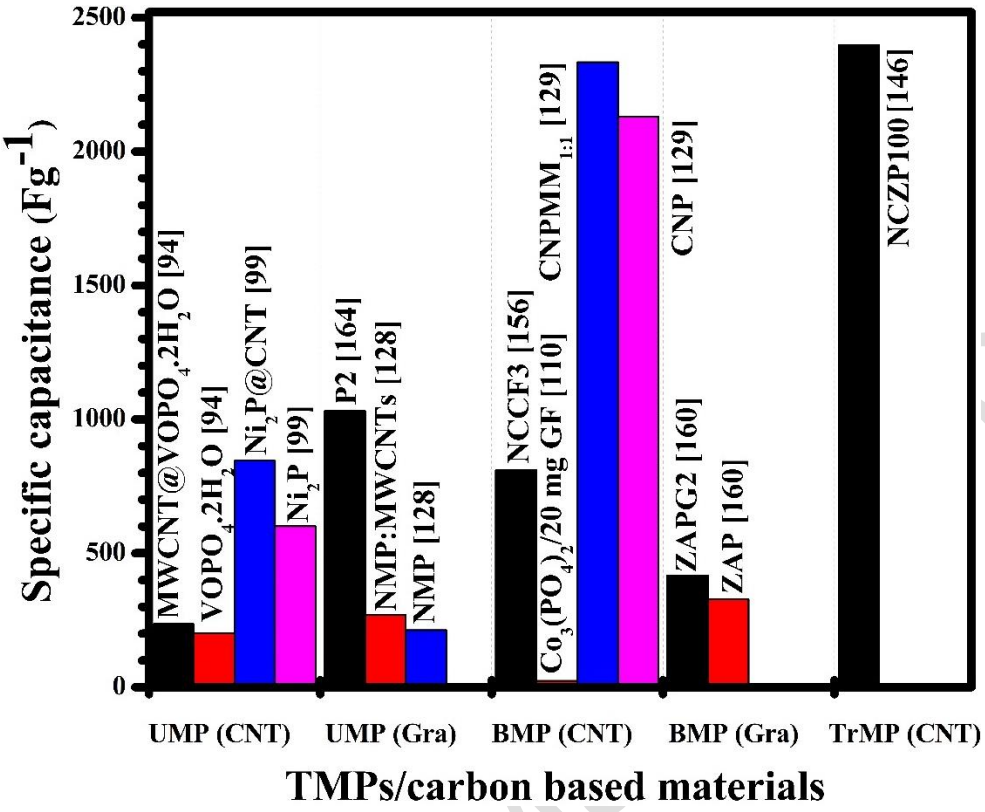

Figure 7: Specific capacity comparison of all TMPs/Carbon based materials and their respective pristine

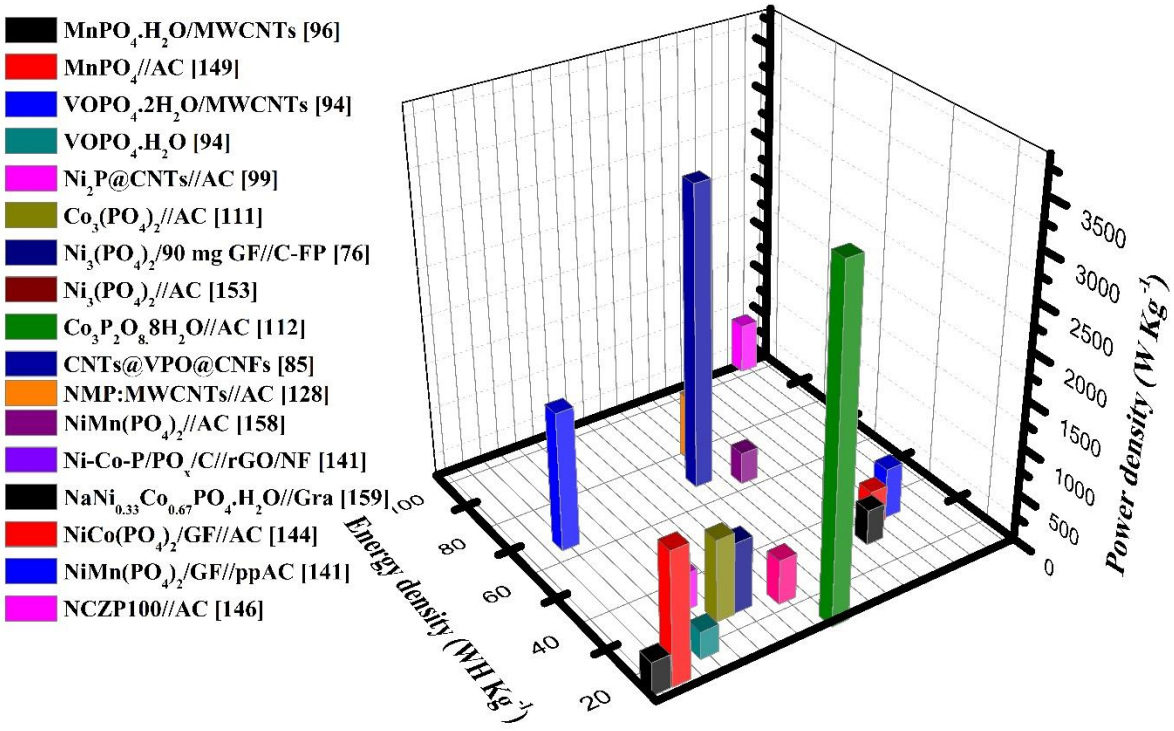

Figure 8: Ragone plot of all previously reported studies

DOI: 10.33961/jecst.2024.00024

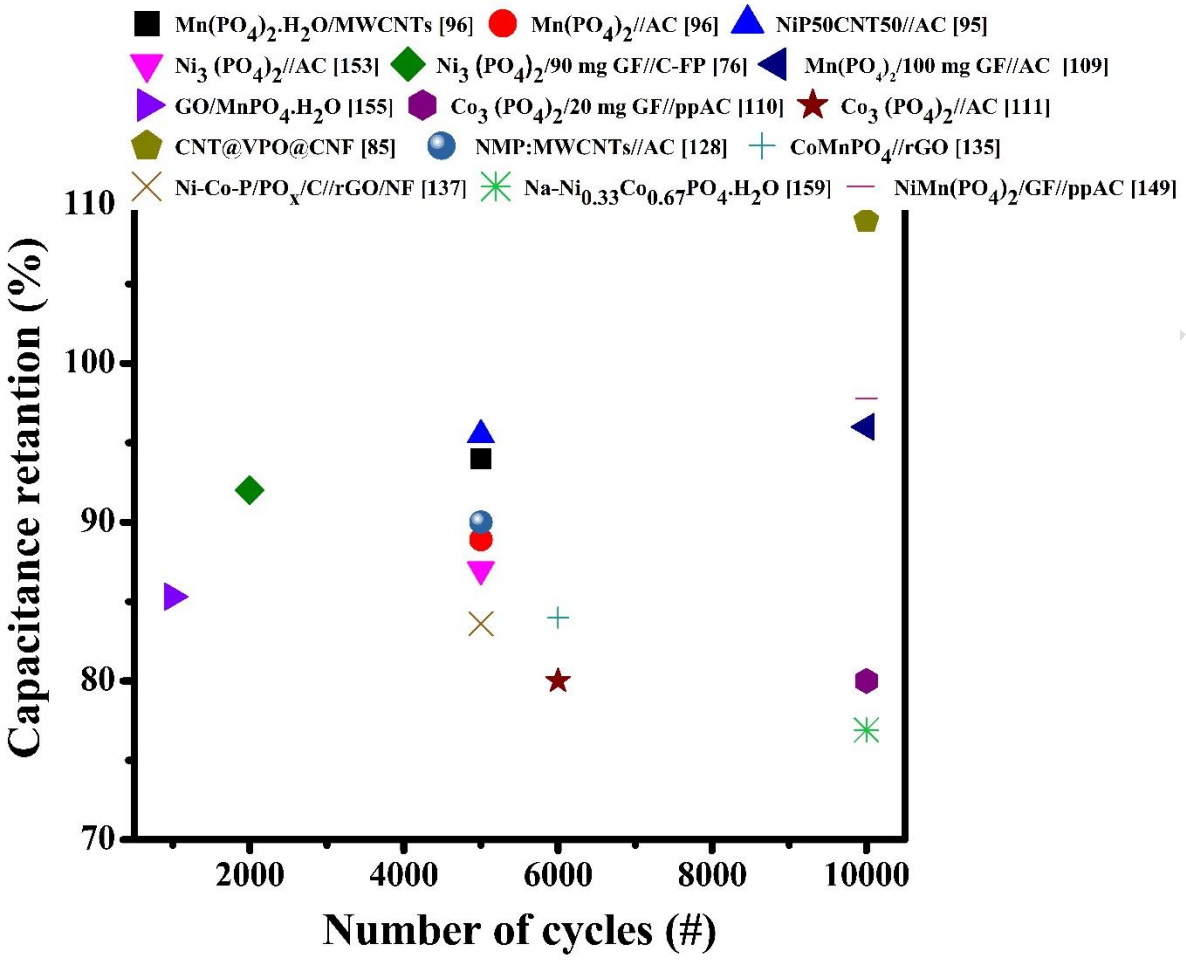

Figure 9: Cyclic performance of all previously reported studies

DOI: 10.33961/jecst.2024.00024

Tables

Table 1: Electrochemical performances of different UMPs and their hybrids with CNTs

Electrode	Synthesis method	Device	Specific capacity ($C\ g^{-1}$)/ capacitance ($F\ g^{-1}$)	Energy density ($Wh\ kg^{-1}$)	Power density ($W\ kg^{-1}$)	Cyclic stability	Ref.
$MnPO_4 \cdot H_2O$/MWCNT	Hydrothermal	-	765	15	350	94 @ 5000 cycles	[96]
MWCNT @ $VOPO_4.\ 2H_2O$	Vaccum filtering	-	236	65.6	1476	-	[93]
Ni_2P @ CNT	Microwave irradiation	Ni_2P @ CNT //AC	854	33.5	387.5	84 @ 5000 cycles	[99]
CNTs @ VPO @ CNFs	Carbonization	CNTs @ VPO @ CNFs SSCD	576.1	69.1	3200	109 @ 10000 cycles	[85]
NiP50CNT50	Sonochemical method	NiP50CNT 50//AC	845 (Specific capacity)	94.5	340	95 @ 5000 cycles	[95]

DOI: 10.33961/jecst.2024.00024

Table 2: Electrochemical performances of different UMPs and their composites with graphene

Electrode	Synthesis method	Device	Specific capacity (C g^{-1})/ capacitance (F g^{-1})	Energy density (Wh kg^{-1})	Power density (W kg^{-1})	Cyclic stability (%)	Ref.
$Ni_3(PO_4)_2$/90 mg GF	Hydrothermal	$Ni_3(PO_4)_2$/90 mg GF//C-FP	-	49	499	92 @ 2000 cycles	[76]
$Co_3(PO_4)_2$/20 mg GF	Co-precipitation	$Co_3(PO_4)_2$/20 mg GF//ppAC	57 mAh g^{-1}	52	847	80 @10000 cycles	[111]
$Co_3(PO_4)_2.4H_2O$/GF	Hydrothermal	$Co_3(PO_4)_2.4H_2O$/ GF// C-FP	57 mAh g^{-1}	24	468	99 @ 10000 cycles	[113]
ZnP-rGO	Hydrothermal	rGO//ZnP_rGO	167.2 (Specific capacity)	24.26	510	71 @ 2000 cycles	[108]
NFPy-CNT	Simple stirring	NFPy-CNT// rGO	517 (Specific capacity)	0.08 mWh· cm^{-2}	7.56 mW· cm^{-2}	86 @ 8000 cycles	[161]
Ni–P @ Ni HL/CC	Hydrothermal	Ni–P @ Ni HL/CC-1h//AC	281 (Specific capacity)	27.6	942.8	86 @ 10,000 cycles	[162]
Fe_2O_3 @ GO	Chemical precipitation	Fe_2O_3 @ GO// $Ni_3(PO_4)_2$ @ GO	1392.6	67.2	200.4	88 @ 1000 cycles	[163]
$Ni_3(PO_4)_2$/ rGO-300	hydrothermal-calcination	$Ni_3(PO_4)_2$/rGO-300 //AC	1726	57.4	160	94 @ 1000 cycles	[148]
Amorpho-us nickel phosphate (P2)	Chemical bath deposition	P2 //rGO	~1031	45.3	1500	80 @ 3000 cycles	[164]
Ni_2P-CNFs	Chemical blowing pyrolysis	Ni_2P-CNFs //CNFs	145 mAh g^{-1}	42	413	88 @ 6000 cycles	[165]
$Ni(OH)_2$/ $Ni(PO_3)_2$	Hydrothermal	$Ni(OH)_2$/$Ni(PO_3)_2$//rGO	1477	67	775	81 @ 8000 cycle	[166]
$Mn_3(PO_4)_2$ /100 mg GF	Hydrothermal	$Mn_3(PO_4)_2$/100 mg GF//AC	270	7.6	360	96 @ 10000 cycles	[109]
GO/Mn $PO_4 \cdot H_2O$ nanowire	Hydrothermal	-	288	5.78	9000	85 @ 1000 cycles	[155]

DOI: 10.33961/jecst.2024.00024

Table 3: Electrochemical performances of different BMPs and their composites with CNTs

Electrode	Synthesis method	Device	Specific capacity (C g^{-1})/ Capacitance (F g^{-1})	Energy density (Wh kg^{-1})	Power density (W kg^{-1})	Cyclic stability (%)	Ref.
NZP60	Sonochemical	NZP60// AC	1143	89.2	630	99.86 @ 5000 cycles	[127]
NMP:MWCNTs	Hydrothermal	NMP:MWCNTs //AC	812	78	698	90 @ 5000 cycles	[128]
CDs/NZP-10	Hydrothermal	CDs/NZP-10//AC	1887	33.7	824.9	90.6 @ 6000 cycles	[123]
P-CSs @ Ni_1-Co_2-PNSs	Hydrothermal carbonization	P-CSs@Ni_1-Co_2-PNSs//AC	1040.3	16.5	750	78 @ 20 A g^{-1}	[117]
$FePO_4$-CNTs	Solvothermal	-	20.8 mF cm^{-2}	-	-	-	
N-CNTs@NiCoP/CoP	Hydrothermal	-	152, mAh g^{-1}	-	-	61% @ 30 A g^{-1}	[125]
$CNPMM_{1:1}$	Hydrothermal	-	2334 $mAhg^{-1}$	-	-	-	

DOI: 10.33961/jecst.2024.00024

Table 4: Electrochemical performances of different BMPs and BMPs/Gra composites

Electrode	Synthesis method	Device	Specific capacity (C g^{-1})/ Capacitance (F g^{-1})	Energy density (Wh kg^{-1})	Power density (Wh kg^{-1})	Cyclic stability (%)	Ref.
$NiCo(PO_4)_3$/GF	Hydrothermal	NiCo $(PO_4)_3$/GF//AC	86.4 mAh g^{-1}	34.8	377	95 @ 10000 cycles	[140]
$Ni_{1.38}Co_{1.62}(PO_4)_2 \cdot 8H_2O$	Binder-free CBD method	$Ni_{1.38}Co_{1.62}(PO_4)_2 \cdot 8H_2O$ //rGO	446 (specific capacity)	36.2	160	83.7 @ 4000 cycles	[167]
ZAPG2	Microwave synthesis	ZAPG2//rGO	416	59.9	153.4	89.4 @ 5000 cycles	[160]
Ni-Co-P/POx/C	Low-temperature phosphating method.	Ni-Co-P/POx/C//rGO/ NF	583 (specific capacity)	37.59	800	83.6 @ 5000 cycles	[137]
CG-CNT	Hydrothermal carbonization	CGCNT_P800 //AGCNT_P800	133	10	-	93 @ 10,000 cycles	[143]
$NiMn(PO_4)_2$/GF	Hydrothermal	$NiMn(PO_4)_2$/GF//ppAC	97 mAh g^{-1}	35.42	538	97.8 @ 10,000 cycles	[141]

DOI: 10.33961/jecst.2024.00024

Table 5: Effect of hierarchical structure, surface area, and porosity of different TMPs

Material	Morphology	Surface area ($m^2 g^{-1}$)	Pore size (nm)	Ref.
MnPO 4·H_2O/MWCNT	Nanosheets	19.6 m2/g	20	[96]
$MnPO_4$·H2O		11.8	17.5	
$Ni_3(PO_4)_2$	-	16.96	-	[147]
NiP50CNT50	-	32.4	-	[95]
NiPH-120	Hollow microsphere	175.5	6..33	[161]
NiP-600		72.1	7.12	
$Ni_3(PO_4)_2$/rGO-300	$Ni_3(PO_4)_2$ particles on rGO nanosheets	198.72	2-10	[148]
NMP:MWCNTs	amorphous NMP balls covered with MWCNT	285.4	13.2	[128]
NMP	Amorphous balls	209.2	18	
CNP	Flower like micro hexagonal structure	5.3	8.7	
$CNPMM_{1:1}$	Flower like micro cuboid structure	11.7	29.4	[131]
$NiCo(PO_4)_3$	Nanoplatelets	2.9		
$NiCo(PO_4)_3$/GF	Nanoplatelets on graphene sheets	6.1	1-18	[140]

DOI: 10.33961/jecst.2024.00024